Generation of functional posterior spinal motor neurons from hPSCs-derived human spinal cord neural progenitor cells

Jax H. Xu[1,7,9], Yao Yao[1,7,9], Fenyong Yao[2,9], Jiehui Chen[1,7,9], Meishi Li[3,7,9], Xianfa Yang[1,4,7], Sheng Li[1,8], Fangru Lu[3], Ping Hu[1,4,6,7,8], Shuijin He[2,*], Guangdun Peng[3,5,6,7,*], Naihe Jing[1,4,6,7,10,*]

[1] State Key Laboratory of Cell Biology, CAS Center for Excellence in Molecular Cell Science, Shanghai Institute of Biochemistry and Cell Biology, Chinese Academy of Sciences, Shanghai, 200031, China

[2] School of Life Science and Technology, ShanghaiTech University, Shanghai 201210, China

[3] Center for Cell Lineage and Development, CAS Key Laboratory of Regenerative Biology, Guangdong Provincial Key Laboratory of Stem Cell and Regenerative Medicine, GIBH-HKU Guangdong-Hong Kong Stem Cell and Regenerative Medicine Research Centre, Guangzhou Institutes of Biomedicine and Health, Chinese Academy of Sciences, Guangzhou 510530, China

[4] Guangzhou Laboratory, Guangzhou, 510005, China

[5] Center for Cell Lineage and Atlas, Bioland Laboratory, Guangzhou, 510005, China

[6] Institute for Stem Cell and Regeneration, Chinese Academy of Sciences, Beijing, 100101, China

[7] University of Chinese Academy of Sciences, Beijing, China

[8] Xinhua Hospital affiliated to Shanghai Jiao Tong University School of Medicine, Shanghai, 20023, China

[9] These authors contributed equally

[10] Lead Contact

* Correspondence: heshj@shanghaitech.edu.cn (S.H.), peng_guangdun@gibh.ac.cn (G.P.), njing@sibcb.ac.cn (N.J.)

SUMMARY

Spinal motor neurons deficiency results in a series of devastating disorders such as amyotrophic lateral sclerosis (ALS), spinal muscular atrophy (SMA) and spinal cord injury (SCI). These disorders are currently incurable, while human pluripotent stem cells (hPSCs)-derived spinal motor neurons are promising but suffered from low-efficiency, functional immaturity and lacks of posterior cellular identity. In this study, we have established human spinal cord neural progenitor cells (hSCNPCs) via hPSCs differentiated neuromesodermal progenitors (NMPs) and demonstrated the hSCNPCs can be continuously expanded up to 40 passages. hSCNPCs can be rapidly differentiated into posterior spinal motor neurons with high efficiency. The functional maturity has been examined in detail. Moreover, a co-culture scheme which is compatible for both neural and muscular differentiation is developed to mimic the neuromuscular junction (NMJ) formation *in vitro*. Together, these studies highlight the potential avenues for generating clinically relevant spinal motor neurons and modeling neuromuscular diseases through our defined hSCNPCs.

INTRODUCTION

Spinal motor neurons (MNs) which directly control muscle contractions are located in the ventral horn of spinal cord and are distributed across the anterior-posterior (AP) axis of the spinal domains from cervical, thoracic, lumbar to sacral (Kanning et al., 2010; Sockanathan and Jessell, 1998). MNs loss results in a spectrum of devastating disorders such as amyotrophic lateral sclerosis (ALS) and spinal cord injury (SCI) (Clowry et al., 1991; Narasimhan, 2006; Nijssen et al., 2017). However, *in vitro* production of spinal MNs and using MNs for drug discovery and disease modeling are hindered due to the inefficient MNs differentiation or inappropriate posterior identity.

Human pluripotent stem cells (hPSCs), including human embryonic stem cells (hESCs) and human induced pluripotent stem cells (hiPSCs), have the potential to generate various cell types *in vitro* and hold promise for disease modeling and cell-replacement therapies (Ebert and Svendsen, 2010; Karagiannis et al., 2019; Takahashi et al., 2007; Thomson et al., 1998; Yu et al., 2007). Many motor neuron differentiation protocols have been developed over the past decades (Ben-Shushan et al., 2015; Cutarelli et al., 2021; Du et al., 2015; Hudish et al., 2020; Lee et al., 2007; Li et al., 2005; Li et al., 2008; Patani et al., 2011; Qu et al., 2014). Generally, hPSCs were firstly induced to form neuroepithelial (NE) cells at embryonic body (EB) or monolayer culture, subsequently specified to OLIG2 positive motor neuron progenitors (MNPs) under the activation of retinoic acid (RA) and sonic hedgehog (SHH). These procedures require 3-4 weeks to differentiate hPSCs into MNPs and another 1-2 weeks to differentiate MNPs into immature MNs, in total 8-10 weeks to generate mature MNs from hPSCs. Alternatively, hPSCs and human fibroblasts can be converted into MNs within 2-3 weeks by forcing the expression of MN inducing transcription factors (Hester et al., 2011; Son et al., 2011). Of note, these inductions of motor neurons from hPSCs predominantly produce cells of mixed hindbrain/cervical axial identities, but are inept in generating high numbers of more posterior thoracic/lumbosacral spinal cord

motor neurons, which are in most cases of key targets of disease and injury.

Spinal motor neuron development initiates from gastrulation, then epiblast cells under dramatic proliferation, differentiation and migration to form three germ layers along the AP axis (Lu et al., 2001; Solnica-Krezel, 2005; Tam and Behringer, 1997). However, the mechanism of AP patterning during the development of the central nervous system (CNS) remains obscure. *In vivo* transplantation experiments of chick embryos revealed that the nodes exhibited disparate competency at different embryonic stages for posterior nervous system induction (Storey et al., 1992). Besides, evidence from mutant T-box gene *Tbx6* in mouse embryos showed that *Tbx6* absent cells switched their cell fates from posterior somites into neuronal cells and formed three neural tube-like structures (Chapman and Papaioannou, 1998). Cell lineage segregation study by clonal analysis in early mouse embryos further indicated that trunk neural ectoderm and neighboring mesoderm derivatives share a common progenitor, namely neuromesodermal progenitor (NMP) (Tzouanacou et al., 2009). NMPs are localized in the caudal lateral epiblasts (CLE) of E8.5 mouse embryos, and express both *Sox2* and *Brachyury (T)* (Henrique et al., 2015). Based on these developmental trajectories, mouse and human NMPs were generated from mESCs and hPSCs and can be differentiated into neural and mesodermal cells *in vitro* (Davis-Dusenbery et al., 2014; Gouti et al., 2014; Turner et al., 2014; Wind et al., 2021). The chromatin accessibility assay showed that the regionalization mechanism along the AP axis during neural induction supports the dual origin of CNS, i.e., the brain and posterior spinal cord are generated from distinct progenitor populations (Metzis et al., 2018). Methods have been established to derive spinal motor neurons through NMPs. For example, Verrier and colleagues established a protocol to rapidly and reproducibly induce human spinal cord progenitors from NMPs-like cells, but these cells and their derivatives only expressed anterior spinal cord markers such as *HOXB4*, *HOXC6* and *HOXA7* (Verrier et al., 2018). Moreover, transplantation of spinal cord neural stem cells derived from hPSCs through NMP-stage showed functional recovery in SCI rat models (Kumamaru et al., 2018).

Nevertheless, only about 50% of these NMP-like cells expressed both SOX2 and Brachyury (T). Thus, the establishment of high-purity human spinal cord neural progenitor cells (hSCNPCs) that are readily attainable for efficient differentiation of posterior spinal motor neurons remains unresolved.

In this study, we established a protocol to generate hSCNPCs from hPSCs through high-purity human NMPs. hSCNPCs showed molecular properties of spinal cord and were readily passaged up to 40 times *in vitro*. These hSCNPCs could be further differentiated into homogeneous spinal motor neurons, and exhibited posterior spinal cord identities. The spinal motor neurons after quick functional maturation could form neuromuscular junction (NMJ) like structures when co-cultured with muscle fibers.

RESULTS

Generation and characterization of human spinal cord neural progenitor cells from hPSCs

To generate NPCs with spinal cord property and posterior regional identity from hPSCs, we mimicked the posterior spinal cord development *in vitro* by differentiating hPSCs into hSCNPCs through high-purity human NMPs (Figure 1A). Feeder-free cultured hESCs were dissociated into single cells, seeded at 40,000 cells/cm^2 and maintained in mTeSR medium for one day to form small clusters, then differentiated in N2B27 medium containing dual-SMAD inhibitors, FGF2 and CHIR99021 for another 3 days. High-purity human NMPs with 90% efficiency were obtained at day 4 (D4) by detecting SOX2 and Brachyury (T) double positive cells (Figures 1B and 1C). CDX2, another NMP marker was also highly expressed in hESCs-derived human NMPs (Figure S1A). To further investigate the molecular profiles of human NMPs, we performed bulk RNA sequencing on samples collected on each day from D0 to D4 and compared our NMPs with previously reported human NMPs, which were isolated by NKX1-2::GFP cell

sorting (Verrier et al., 2018). Principal component analysis (PCA) demonstrated a clear differentiation trajectory from hESCs to human NMPs, and showed a high correlation between the D4-hNMPs with NKX1-2 enriched human NMPs (Figure 1D), suggesting that this protocol represents a new route to NMP generation.

Next, high-purity human NMPs were subjected to hSCNPCs differentiation. At D4, human NMPs were dissociated into single cells and replated with a seeding density of 100,000 cells/cm^2 in neural determination medium (NeuDet), which contains dual-SMAD inhibitors, FGF2, FGF8, CHIR99021 and Compound E for another 6 days (Figure 1A). Real-time quantitative PCR (RT-qPCR) analysis showed that the pluripotent gene *POU5F1* and human NMP marker gene *NKX1-2* were downregulated, while *CDX2* and neural progenitor marker genes *SOX2*, *PAX6* and *NKX6-1* and HOX family genes of posterior identity such as *HOXC9* and *HOXC10* were upregulated (Figure S1D). By day 10 (D10), these hSCNPCs can be passaged in medium containing Purmorphamine, SB431542 and CHIR99021 over 40 times *in vitro* with normal karyotype (Figures 1A, 1E and S1E). Immunofluorescent staining showed that hSCNPCs expressed high percentage of pan-NPC markers NESTIN, SOX1, SOX2 and PAX6 (Figures 1F and 1G), as well as expressed moderate level of proliferation marker KI67 and spinal cord specific markers, such as NKX6-1 (~60%), NKX2-2 (~30%) and OLIG2 (~5%) (Figures 1F and 1G). Human iPSCs can also be differentiated into hiSCNPCs through hiNMPs with the same protocol, indicating the robustness of this method (Figures S1B, S1C and S1F).

To further determine the dynamic changes from hESCs to hSCNPCs at the transcriptomic level, we performed bulk RNA sequencing during NeuDet stage and hSCNPCs at different passages. PCA analysis based on regulon expression showed that three major cell groups, hNMPs, differentiating neural progenitors and passaged hSCNPCs, were aligned in a timely order (Figure 1H). Regulon analysis showed that hNMPs mainly enriched with Gene Ontology (GO) terms of cell cycle process, Wnt signaling pathway and fibroblast growth factor receptor signaling pathway; NeuDet

stage differentiating neural progenitors mainly enriched with stem cell differentiation and spinal cord development; passaged hSCNPCs enriched mainly with anterior/posterior pattern specification and neural precursor cell proliferation (Figure 1I). Interestingly, we observed a caudalized shift of HOX genes expression from *HOXC6-8* at NeuDet stage to *HOXC9-10* in passaged hSCNPCs (Figure 1I), suggesting an enhanced posterior signature during the derivation process. Comparison of the transcriptome of our hSCNPCs with that of human developing brain (Allen Brain Atlas) and human developing spinal cord (Rayon et al., 2021) confirmed that hSCNPCs are resembling to human developing spinal cord (Figure 1J).

Taken together, these results suggest that we have successfully obtained a neural progenitor cell line with human spinal cord features.

Fast and direct differentiation of posterior spinal motor neurons from hSCNPCs

To test the motor neuron differentiation ability of hSCNPCs, we dissociated hSCNPCs into single cells and seeded with a density of 100,000 cell/cm^2 on PDL and Matrigel-coated plates and differentiated in N2B27 medium containing Purmorphamine, Compound E, brain-derived neurotrophic factor (BDNF), glial cell line-derived neurotrophic factor (GDNF) and Neurotrophin-3 (NT-3) (Figure 2A). In this medium, hSCNPCs can be quickly differentiated into immature motor neurons expressed markers of HB9 (~90%) and ISL1 (~70%) at day 6 (D6) (Figures 2B and 2D). By day 18 (D18), hSCNPCs-derived motor neurons expressed homogeneously mature neuronal markers, such as SMI-32 (~90%), NEUN (~90%) and MAP2 (~90%) (Figures 2C and 2D). These cells also expressed motor neuron subtype-specific markers, such as choline acetyltransferase (ChAT) and vesicular acetylcholine transporter (VAChT) at high percentages (Figures 2E and 2F). Other neuronal subtypes, such as glutamatergic neurons (VGLUT), GABAergic neurons (GAD67) and dopaminergic neurons (TH), were barely detectable (Figures 2E and 2F), suggesting that this method is a highly efficient spinal motor neuron differentiation protocol.

HOX genes play an important role in the rostrocaudal axis and spinal cord patterning, immunostaining analysis showed that hSCNPCs-derived spinal motor neurons mainly expressed HOXC9 (~70%) and HOXD11 (~30%), which were associated with thoracic and lumbar spinal domains, respectively (Figures 2G and 2H). The regional identities of hindbrain (HOXB4), cervical spinal (HOXC6) and lumbar spinal cord (HOXD10) were hardly detectable (Figures 2G and 2H). To further illustrate the expression patterns of *HOX* family genes during spinal motor neuron differentiation, we profiled 4 *HOX* clusters of 39 genes in the RNA-seq data. In line with the immunostaining results, spinal motor neurons generated from hSCNPCs specifically expressed *HOXC9* (Figure 2J). Together, these results suggest that the motor neurons this protocol induced are the posterior spinal motor neurons.

Similarly, the motor neurons derived from hiPSCs through hiSCNPCs using the same protocol also showed comparable expression levels of spinal motor neuron markers and HOX proteins (Figure S2B).

To gain insights into the transcriptomic alterations during spinal motor neuron differentiation, we employed time course RNA-seq analysis every 6 days from D0 to D30, as well as D42. The SCENIC algorithm identified 252 regulons (Figure S2C) and the PCA analysis showed a turning point at D6 (Figure 2I). Heatmap and GO term analysis showed that D0-D6 regulons were enriched with terms of spinal cord patterning, cell cycle DNA replication and neural precursor cell proliferation, and regulons of late stage were corresponding to neuron migration, neural tube formation, neuromuscular junction development and neurotransmitter secretion (Figure S2C). Hence, the spinal motor neuron differentiation process could be divided into two major events: motor neuron differentiation and maturation. We observed temporal activation of transcription factors that may account for the cell fate transition of hSCNPCs, for example, *JUN*, *GBX2*, *FOXP2*, *ONCUT3* and *SIX3* (Figure S2C). We also confirmed by RT-qPCR that the expression of NPC marker genes *NESTIN* and *NKX2-2* were downregulated, while motor neuron progenitor specific marker *NKX6-1* increased from

D0 to D18 and remained the expression level thereafter, indicating that *NKX6-1* may play an important role during motor neuron fate determination and maintenance; the expression of immature neuronal marker *TUJ1* increased sharply from D0 to D6, then dramatically decreased and maintained a relatively low level; and immature motor neuron markers *HB9* and *ISL1* increased from D0 to D12 then slowly decreased (Figure S2A). In contrast, the expression of mature neuronal marker *NEUN* and mature motor neuron markers *ChAT* and *VAChT* increased from D0 to D12, and were maintained afterwards (Figure S2A).

To test whether hSCNPCs have the potential to give rise to other cell types of the spinal cord, we applied a spontaneous differentiation system to hSCNPCs. hSCNPCs were plated as single cells and differentiated in N2B27 medium without additional patterning factors. In this condition, hSCNPCs differentiated into mature neurons with centimeter-long axon bundles (Figures S2D and S2E). MicroRNA-218 (mir-218) was previously reported as an authentic marker of both rodent and human motor neurons (Amin et al., 2015; Amin et al., 2021; Hoye et al., 2018; Reichenstein et al., 2019). To compare the difference between spinal motor neurons and spontaneous differentiated neurons, time course RT-qPCR was performed for samples from both systems every 3 days from D0 to D21. The results showed that *mir-218-2* was specifically elevated in cells from spinal motor neuron differentiation system (Figure S2F). Albeit the much lower efficiency of motor neuron differentiation, we still detected HB9 positive cells in spontaneous culture. Interestingly, interneuron markers GABA and Somatostatin (SST) and astrocyte marker S100β were also presented in spontaneous differentiation (Figure S2G), indicating that hSCNPCs as neural progenitors have the capacity to generate the major neural cell lineages of spinal cord.

Functional characterization of posterior spinal motor neuron derived from hSCNPCs

To characterize the functional maturation of the posterior spinal motor neurons, we

253 performed whole-cell patch-clamp and CMOS-based high-density microelectrode array
254 (HD-MEA) recordings. Spinal motor neurons co-cultured with astrocytes exhibited a
255 mature morphology with abundant dendrites and long axons, and expressed mature
256 motor neuron marker SMI-32 (Figures S3A and S3B). The action potentials (APs) were
257 examined during 42 days of spinal motor neuron differentiation by whole-cell patch-
258 clamp (Figure 3A). In response to a series of step current injections, 20% neurons could
259 quickly generate single spike at D6 of differentiation and the mean amplitude was 24.12
260 ± 6.39 mV. After 12 days of differentiation, 50% neurons fired trains of APs and the
261 mean amplitude was 41.27 ± 3.53 mV. At day 18, near 80% neurons fired repetitive APs
262 at a mean amplitude of 47.76 ± 3.27 mV. As maturation progressively increased, 100%
263 of recorded neurons showed sharp and repetitive spikes at 24 days, 30 days and 42 days
264 of differentiation with mean amplitudes of 67.77 ± 2.69 mV, 71.91 ± 2.52 mV and 69.14
265 ± 2.63 mV, respectively (Figures 3A-3C and S3C). Statistical analysis of AP thresholds
266 and resting membrane potentials (RMPs) showed that the mean values of AP thresholds
267 and RMPs became more negative as the *in vitro* culture proceeded and reached a plateau
268 after 24 days of spinal motor neuron differentiation at -32.15 ± 1.14 mV and -48.73 ±
269 1.12 mV, respectively (Figures 3D and 3E). A gradual reduction from ~1 GΩ to ~0.5
270 GΩ of input resistance (Rin) was also observed during spinal motor neuron maturation
271 (Figure 3F). The F-I curves of spinal motor neurons from D6 to D42 exhibited a gradual
272 increase in spike frequency under the increasing current injections from 0 pA to 30 pA
273 and reached a plateau under the current injection over 30 pA (Figure 3G). Together,
274 whole-cell patch-clamp recordings reveal that hSCNPCs-derived spinal motor neurons
275 exhibit a fast maturation property at 24 days of differentiation, and show the highest
276 electrophysiological function at D30 and then under a slight degeneration at D42 of
277 differentiation.

278 To comprehensively investigate the maturity of spinal motor neurons, we utilized the
279 CMOS-based HD-MEA platform, which is a high-throughput and high-resolution
280 system containing 26,400 electrodes and 1,024 simultaneous recording channels

(Muller et al., 2015; Sundberg et al., 2021; Yuan et al., 2020). We first scanned and analyzed the entire HD-MEA electrode array to examine spontaneous neural activities during spinal motor neuron differentiation. The percentage of active electrodes rose rapidly from D6 to D18 and then was stabilized at about 75% thereafter (Figure 3H). The presented heatmaps of firing rate over the time course differentiation from D6 to D42, and statistical analysis of mean firing rate (MRF) showed that the time span for functional maturity is from D18 to D42, which is consistent with whole-cell patch-clamp results (Figures 3C and 3I). Then, axon tracking and spike sorting assays were performed to depict the functional images of axons and neurites of single neurons during spinal motor neuron differentiation (Figure 3J). We assessed the axon tracking metrics including mean neuron conduction velocity (m/s), mean total axon length (μm), mean longest branch length (μm), mean longest distance from initiation site (μm) and mean longest latency (ms). These results showed that all of the parameters described above were steadily increased accompanying the differentiation progresses, pointing to a step-wise electrophysiological maturation of the spinal motor neurons (Figure 3K).

Neural networks or neural circuits are featured by synchronous signals which are based on connections between pre- and postsynaptic neurons. To assess the neural network properties of spinal motor neurons, we performed network analysis during differentiation. No synchronous burst was observed from D6 to D42 after differentiation, while network oscillations were demonstrated in cortical neurons differentiated from iNSCs previously generated in our lab (Zhang et al., 2019) (Figure 3L). Moreover, we also used whole-cell patch-clamp to record spontaneous postsynaptic currents (sPSC) of spinal motor neurons at D30 of differentiation and no sPSC were recorded (Figure S3D). Although the spinal motor neurons can produce robust and abundant single burst (data not shown), they were yet to form microcircuit assembly under an *in vitro* culture system. We reasoned that the spinal motor neurons derived from hSCNPCs are of high purity and were not able to form synapses without other cell types. To test this hypothesis, immunofluorescent staining of pre- and

postsynaptic markers synaptophysin (SYP) and PSD95 was performed to characterize synapse formation. The results showed that hSCNPCs-derived spinal motor neurons expressed only presynaptic marker synaptophysin but not postsynaptic marker PSD95, while iNSCs differentiated cortical neurons expressed them both (Figure 3M).

Taken together, both whole-cell patch-clamp and CMOS-based HD-MEA results reveal that hSCNPCs differentiated spinal motor neurons exhibit a fast mature property from D18 onward.

Generation and characterization of 3D spinal motor neuron spheroids from hSCNPCs

Spinal motor neurons aggregate to form motor columns and pools in the spinal cord during vertebrate development, of which the somata reside in the spinal cord while the axons extend out to target muscles (Dasen et al., 2005; De Marco Garcia and Jessell, 2008; Guthrie, 2004). In order to mimic *in vivo* spinal motor neuron aggregates and neuron-muscle interaction *in vitro*, we generated three-dimensional (3D) spinal motor neuron spheroids from hSCNPCs and tried to find the suitable conditions for co-culture spinal motor neurons with muscle cells. Single hSCNPCs suspension was prepared and seeded in V-bottom 96-well plates at 50,000 cells/well to differentiate into 3D spinal motor neuron spheroids in the presence of Purmorphamine, Compound E, BDNF, GDNF, NT-3 and CultureOne^{TM} supplement in N2B27 medium (Figure 4A). Time course RT-qPCR showed that the expression levels of spinal cord neural progenitor marker genes *NESTIN*, *NKX2-2* and immature motor neuron marker genes *TUJ1*, *HB9* and *ISL1* declined in this 3D differentiation system; on the contrary, the expression of mature spinal motor neuron marker genes *NEUN*, *ChAT* and *VAChT* gradually increased until D12 (Figure 4B). To further confirm the spinal motor neuron feature, maturity and regional identity of 3D spinal motor neuron spheroids at D12 of differentiation, we performed immunofluorescent staining of cryosection spheroids at D12. The results showed that hSCNPCs-derived 3D spinal motor neuron spheroids homogeneously

337 expressed motor neuron markers HB9 and SMI-32, mature neuronal markers NEUN
338 and MAP2 and mature motor neuron markers ChAT and VAChT (Figures 4C and 4D).
339 For regional identity, many cells (~60%) of spinal motor neuron spheroids expressed
340 HOXC9, but no cell expressed HOXB4 (Figures 4E and 4F). Collectively, these results
341 suggest that the suitable time for spinal motor neuron spheroids to co-culture with
342 muscle cells is at differentiation D12.
343
344 **Formation pattern of complex and pretzel-shaped acetylcholine receptor**
345 **aggregates during C2C12 myogenic differentiation**
346 One of the most important roles of spinal motor neurons is to form neuromuscular
347 junctions (NMJs) with targeted muscles, leading to muscle innervation. To model NMJ
348 formation *in vitro* with hSCNPCs-derived spinal motor neurons, a robust and
349 reproducible co-culture system of spinal motor neurons and skeletal muscles is a
350 prerequisite. To obtain an optimized myotube differentiation condition, we tested four
351 combinations of different cell seeding densities and durations of propagation stage, then
352 differentiated the cells for another 6 days (Figure S4A). Immunofluorescent staining of
353 mature muscle fiber marker myosin heavy chain (MyHC) and fluorescent α-
354 bungarotoxin (α-BTX) staining showed that C2C12 cells differentiated into the most
355 complex structure and the highest numbers of AChR clusters with an initial seeding
356 density of 40,000 cells/cm^2 and 2 days propagation (Figures S4B and S4C). Thus, we
357 established a differentiation protocol to proliferate C2C12 cells in propagation medium
358 containing 10% FBS-DMEM for 2 days and subjected these cells to differentiate for 14
359 days with 2% horse serum (HS) (Figure 5A). Immunostaining analysis showed that
360 AChR accumulated into small plaques at day 4 of myogenic differentiation, which
361 became branched forms and pretzel-like shaped clusters at day 6, and then diffused
362 along the myotubes at day 8 (Figures 5B and S4C). We also quantified the fiber length,
363 fiber width, nuclei numbers per fiber, MyHC surface area, AChR area and the ratio of
364 AChR to MyHC. The results showed that C2C12 fused into myotube and gradually

matured to form muscle fibers from day 0 to day 6, and then degenerated afterwards (Figure 5C).

Taken together, we have established a protocol to differentiate C2C12 into mature muscle fibers with abundant and pretzel-shaped aneural AChR clusters.

Co-culture spinal motor neuron spheroids and C2C12-derived muscle fibers to form NMJ-like structures *in vitro*

After obtaining the proper differentiation conditions for muscle cells and spinal motor neuron spheroids, we next sought to find a suitable condition to co-culture these two types of cells to model the NMJ formation *in vitro*. To this end, we first attempted to determine the co-culture medium by testing different combinations of basal medium (DMEM or N2B27), chemical additives (with or without supplementation of Purmorphamine and Compound E (P/E)) and serum (horse serum (HS) or Ultroser^{TM} G serum substitute (UG)). Having separately cultured these two types of cells in these different co-culture media for 2 days, we found that 0.2% UG and DMEM medium supported both 3D spinal motor neuron spheroids differentiation and C2C12 myotube fusion more efficiently than the other conditions, and Purmorphamine or Compound E showed no additive effect (Figures 6A and 6B). Furthermore, RT-qPCR confirmed that mature motor neuron marker genes *NEUN*, *VAChT* and *ChAT* and AChR associated markers *musk*, *chrng* and *chrne* were highly expressed in this condition (Figures 6C and 6D). Hence, we have obtained a co-culture medium that facilitates both motor neuron and myogenic differentiation.

To co-culture motor neurons and muscle cells, we added differentiation day 12 spinal motor neuron spheroids onto day 4 muscle fibers derived from C2C12 myogenic differentiation, then cultured them in the DMEM medium supplemented with 0.2% UG for 2 days (Figure 6E). Immunostaining analysis showed that spinal motor neuron spheroids extended neurites following the orientations of muscle fibers (Figure 6F), indicating that muscle fibers may have a guiding cue on axonal growth of motor neurons.

Furthermore, MyHC, TUJ1 and α-BTX co-staining showed that NMJ-like structures were formed *in vitro* after co-culturing hSCNPCs-derived 3D spinal motor neuron spheroids with C2C12-derived muscle fibers for 2 days (Figure 6G).

Taken together, we have established a co-culture system, in which both spinal motor neurons and muscle cells could differentiate to maturation and form NMJ-like structures *in vitro*.

DISCUSSION

In this study, we differentiated hPSCs into self-renewal hSCNPCs through human NMPs. These neural progenitor cells express homogeneous pan-NPC markers as well as spinal cord specific markers and can be passaged over 40 times *in vitro*. The hSCNPCs could be further differentiated into high-purity motor neurons with posterior spinal cord regional identity. The spinal motor neurons derived from hSCNPCs could be electrophysiologically mature after long-term differentiation. Moreover, co-culture of hSCNPCs-derived spinal motor neurons with C2C12-derived muscle fibers could form NMJ-like structures *in vitro*.

There is enormously regional diversity in the central nervous system. Conventionally, the generation of regional specific NPCs from hPSCs follows a general principle of neural development, hypothesized as an “activation transformation” paradigm. This model proposes that cells first undergo neural induction (“activation”) to form default anterior neural fates and caudal regions of motor neurons are generated by induction under caudalising signals such as RA and ventralizing factor SHH (“transformation”) (Mangold, 1933; Nieuwkoop and Nigtevecht, 1954; Stern, 2001). *In vitro* stepwise differentiation of motor neuron progenitors (MNPs) commonly contains two major steps. hPSCs are first differentiated into neuroepithelial (NE) cells within two weeks, then NE cells are specified to MNPs in the presence of RA and SHH (Du et al., 2015;

Hu and Zhang, 2009; Lee et al., 2007; Li et al., 2005). Meanwhile, dual-SMAD inhibitors are used to increase the differentiation efficiency of NE cells and shorten the differentiation time (Chambers et al., 2009). However, the most caudal markers characterized in those studies are relative to hindbrain and cervical region of anterior spinal cord (Sances et al., 2016). Mechanistic studies also reveal that RA treatment leads to the binding of retinoic acid receptors (RARs) to *Hox1-5* chromatin domains (Mahony et al., 2011; Mazzoni et al., 2013). Increasing evidences have indicated that posterior spinal cord has a distinct developmental origin from NMPs (Gouti et al., 2014; Metzis et al., 2018; Tzouanacou et al., 2009). Human spinal cord neural stem cells have been generated from hPSCs through a transient stage of NMP, but the efficiency of SOX2 and Brachyury (T) double positive NMPs is only around 50% (Kumamaru et al., 2018), raising the potential safety concerns. In this study, we have optimized human NMPs differentiation system and obtained over 90% efficiency (Figure 1). Importantly, this protocol is stable and reproducible due to optimized seeding density and standard operation procedures which could facilitate its clinical usage. The hSCNPCs can be derived from human NMPs and exhibit spinal cord specific features by expressing NKX6-1, NKX2-2 and OLIG2 with continuously passage property *in vitro* (Figure 1).

As one of the vital cell types in the spinal cord, motor neurons (MNs) are of great clinical importance in spinal cord injury as well as motor neuron diseases such as ALS and SMA (Fujimori et al., 2018; Olmsted et al., 2021; Sances et al., 2016; Wang et al., 2013). Conventionally, differentiation of postmitotic motor neuron has disadvantages in time consumption, low efficiency and particularly incapable of making caudal spinal motor neurons (Hu and Zhang, 2009; Sances et al., 2016). The hSCNPCs based spinal motor neuron differentiation is robust and only takes 18 days to generate ChAT and VAChAT positive mature spinal motor neurons, and these cells express posterior spinal cord HOX markers such as HOXC9 and HOXD11 (Figure 2). Furthermore, the whole-cell patch-clamp and HD-MEA recordings showed that the hSCNPCs-derived spinal motor neurons can fire single AP as early as 6 days of differentiation and over 80% cells

449 can fire APs at day 18. By day 30, the membrane properties of spinal motor neurons
450 reach to the most mature function (Figure 3). HD-MEA analyses also showed a
451 consistent maturation pattern as patch-clamp electrophysiology illustrated (Figure 3).
452 In motor neuron diseases, the core synapse and therapeutic relevant structure is the
453 neuromuscular junction (NMJ) (Kariya et al., 2014; Picchiarelli et al., 2019). *In vitro*
454 modeling of NMJ has been challenging, which demands proper juxtaposition of both
455 spinal motor neuron and skeletal muscle differentiation (Bakooshli et al., 2019; Guo et
456 al., 2011; Martins et al., 2020; Osaki et al., 2020). The established protocols for
457 generating NMJ *in vitro* can hardly form pretzel-shaped NMJ structures. By optimizing
458 the C2C12 differentiation process, we showed that the AChR cluster formation begins
459 at day 4 and degenerates at day 8 of *in vitro* differentiation (Figure 4). Moreover, we
460 also have established a protocol to differentiate hSCNPCs into 3D spinal motor neuron
461 spheroids which can better mimic the positional relation between spinal motor neurons
462 and skeletal muscle fibers (Figure 5). Spinal motor neurons and skeletal muscle fibers
463 favor different culture conditions (Barbeau et al., 2020). For example, muscle fiber
464 differentiation needs horse serum whereas serum does not benefit neural differentiation.
465 Thus, we have systematically screened different co-culture conditions, and have found
466 that DMED medium supplemented with Ultroser^{TM} G serum substitute is most suitable
467 for co-culture of hSCNPCs-derived spinal motor neuron spheroids and C2C12-derived
468 muscle fibers. Finally, we have obtained an efficient co-culture system for spinal motor
469 neurons and skeletal muscles, and reproduced NMJ-like structures *in vitro* (Figure 6).
470 Adult mammals have limited regeneration of CNS, while stem cells-derived NPCs
471 hold promises to restoring functional neural circuits *in vivo* (Varadarajan et al., 2022).
472 Studies of cell transplantation therapy of SCI also provide evidences of motor neuron
473 progenitors on the recovery of locomotor functions (Ceto et al., 2020; Kadoya et al.,
474 2016; Kumamaru et al., 2018; Kumamaru et al., 2019). The hSCNPCs-derived from
475 high-purity NMPs and exhibit spinal cord specific properties, and can be largely
476 expanded to meet the need of high-volume cell transplantation. Besides, the ability to

form NMJ and 3D sophistical structure would facilitate the mechanistic studies of human spinal motor neurons in development and disease. We expect the availability of hSCNPCs will hold great potential for regenerative medicine and translational study.

ACKNOLEDGEMENTS

This work was supported in part by the National Key Basic Research and Development Program of China (2019YFA0801402, 2018YFA0800100, 2018YFA0108000, 2018YFA0107200), "Strategic Priority Research Program" of the Chinese Academy of Sciences, Grant No. (XDA16020501, XDA16020404), National Natural Science Foundation of China (32130030, 31630043, 31871456, 31900454).

AUTHOR CONTRIBUTIONS

J.H.X. and N.J. conceived the project. J.H.X., Y.Y. and M.L performed the experiments and collected the data. J.H.X. and Y.Y. designed the experiments, analyzed the data and made figures. F.Y. performed patch-clamp electrophysiology. X.Y. produced and J.C. analyzed the RNA-seq data. J.H.X., G.P. and N.J. wrote the manuscript. N.J. supervised the study. All authors read and approved the final manuscript.

DECLARATION OF INTERESTS

The authors declare no competing interest.

Main Figures titles and legends

Figure 1. Generation and characterization of human spinal cord neural progenitor cells from hPSCs

(A) Schematic procedure for generating hSCNPCs and hiSCNPCs from hPSCs (H9, DC60-3, DC87-3) with all stages, media and factors.

(B) Immunostaining of hNMPs markers SOX2 and Brachyury (T) at day 4. Scale bar, 50 μm.

(C) Quantification of SOX2 and Brachyury (T) double positive cells over DAPI of hNMPs-D4. n = 4 independent experiments. Data are represented as mean ± SD.

(D) Principal component analysis of time course samples during hNMPs differentiation and the previously published samples of NKX1-2-GFP sorted human nmps (Verrier et al., 2018).

(E) Cumulative growth curve of hSCNPCs counts over 40 passages. n = 2 independent experiments. Data are represented as mean ± SD.

(F) Immunostaining of hSCNPCs (top panel exhibited pan-NPC markers and proliferation marker; bottom panel exhibited spinal cord specific NPC markers). Scale bar, 50 μm.

(G) Quantification of results shown in Figure 1F. n = 5 independent experiments. Data are represented as mean ± SD.

(H) Principal component analysis of samples from hESCs (H9) to hSCNPCs at each time point shown in Figure 1A.

(I) The heat-map showing three regulon groups in samples of hESCs (H9) to hSCNPCs with listing representative regulon transcription factors (numbers of predicted target genes by SCENIC in the brackets) and enriched GO terms for each regulon group.

(J) Comparative analysis of whole transcriptome of hSCNPCs at different passages to dataset from Allen Brain Atlas of developing human brain and previous published dataset of developing human spinal cord.

Figure 2. Fast and high-efficient posterior spinal cord motor neuron differentiation from hSCNPCs

(A) Schematic illustration of direct spinal motor neurons differentiation from hSCNPCs and hiSCNPCs (derived from H9, DC60-3 and DC87-3).

(B) Immunofluorescent images demonstrating the expression of motor neuron markers HB9, ISL1 of hSCNPCs direct differentiated spinal motor neurons at day 6. Scale bar, 50 μm.

(C) Immunofluorescent images demonstrating the expression of mature motor neuron marker SMI-32 and mature neuronal markers NEUN and MAP2 of hSCNPCs direct differentiated spinal motor neurons at day 18. Scale bar, 50 μm.

(D) Quantification of results shown in Figures 2B and 2C. n = 5 independent experiments. Data are represented as mean ± SD.

(E) Immunofluorescent images of neurotransmitter markers ChAT, VAChT, VGLUT, GAD67 and TH of hSCNPCs-derived spinal motor neurons at day 18. Scale bar, 50 μm.

(F) Quantification of results shown in Figure 2E. n = 5 independent experiments. Data are represented as mean ± SD.

(G) Immunofluorescent staining of HOX family genes HOXB4, HOXC6, HOXC9, HOXD10 and HOXD11 of hSCNPCs-derived spinal motor neurons at day 18. Scale bar, 50 μm.

(H) Quantification of results shown in Figure 2F. n = 5 independent experiments. Data are represented as mean ± SD.

(I) Principal component analysis of samples from hSCNPCs to spinal motor neurons at each time point shown in Figure 2A.

(J) 39 HOX genes expression profiles during spinal motor neuron differentiation from hSCNPCs.

Figure 3. Functional characterization of hSCNPCs direct differentiated posterior spinal motor neurons

(A) Representative recording traces of hSCNPCs-derived spinal motor neurons from day 6 to day 42 in response to step current injection.

(B) Percentages of hSCNPCs-derived spinal motor neurons from day 6 to day 42 with AP and no AP. N numbers of technical replicates were shown in figures from 3 independent experiments. Data are represented as mean ± SD.

(C) Quantification of AP amplitude of hSCNPCs-derived spinal motor neurons from day 6 to day 42. N numbers of technical replicates were shown in figures from 3 independent experiments. Data are represented as mean ± SD.

(D) Quantification of AP threshold during hSCNPCs spinal motor neurons differentiation from day 6 to day 42. N numbers of technical replicates were shown in figures from 3 independent experiments. Data are represented as mean ± SD.

(E) Quantification of resting membrane potential (RMP) of hSCNPCs-derived spinal motor neurons from day 6 to day 42. N numbers of technical replicates were shown in figures from 3 independent experiments. Data are represented as mean ± SD.

(F) Quantification of input resistance (Rin) of hSCNPCs-derived spinal motor neurons decreased over the differentiation process. N numbers of technical replicates were shown in figures from 3 independent experiments. Data are represented as mean ± SD.

(G) Comparison of F-I curves from hSCNPCs-derived spinal motor neurons at day 6, day 12, day 18, day 24, day30 and day 42. Data were collected from 3 independent experiments. Data are represented as mean ± SD.

(H) Spatial distribution maps of active spikes and the quantification results during spinal motor neuron differentiation from day 6 to day 42. n = 3 independent experiments. Data are represented as mean ± SD.

(I) Representative mean firing rate and the quantification results during spinal motor neuron differentiation from day 6 to day 42. n = 3 independent experiments. Data are represented as mean ± SD.

(J) Representative axon tracking maps during spinal motor neuron differentiation from day 6 to day 42.

(K) Quantification results of axon tracking during spinal motor neuron differentiation from day 6 to day 42. Data were collected from 3 independent experiments. Data are represented as mean ± SD.

(L) Network analysis during spinal motor neuron differentiation from day 6 to day 42

589 and cortical neuron at day 18 as a positive control.

590 (M) Immunostaining of pre- (SYP, Synaptophysin) and post-synaptic (PSD95) markers

591 of hSCNPCs-MNs and cortical neurons at day 18. Scale bar, 50 μm.

592

593 **Figure 4. Three-dimensional spinal motor neuron spheroids differentiation from**

594 **hSCNPCs**

595 (A) Schematic illustration of the differentiation process of three-dimensional spinal

596 motor neuron spheroids.

597 (B) Fold changes of marker genes expression (relative to the expression level of

598 GAPDH) during 3D spinal motor neuron spheroids differentiation. n = 4 independent

599 experiments. Data are represented as mean ± SD.

600 (C) Immunofluorescent staining of HB9, SMI-32 and NEUN in spinal motor neuron

601 spheroids at day 12 after differentiation. Scale bar, 50 μm.

602 (D) Immunofluorescent staining of MAP2, ChAT and VAChT in spinal motor neuron

603 spheroids at day 12 after differentiation. Scale bar, 50 μm.

604 (E) Immunofluorescent staining of HOXB4 and HOXC9 in spinal motor neuron

605 spheroids at day 12 after differentiation. Scale bar, 50 μm.

606 (F) Statistic analysis and quantification of Figure 4E. n = 3 independent experiments.

607 Data are represented as mean ± SD. Student's t test. P value was presented in the figure.

608

609 **Figure 5. Step-wise myogenic differentiation of C2C12**

610 (A) Schematic procedure of C2C12 differentiation.

611 (B) Immunostaining of muscle fiber marker (MyHC) and AChR during muscle fiber

612 differentiation of C2C12 from day 0 to day 14. Scale bar, 50 μm.

613 (C) Quantification results of Figure 5B. Data were collected from 3 independent

614 experiments. Data are represented as mean ± SD.

615

616 **Figure 6. Co-culture of hSCNPCs-derived spinal motor neuron spheroids and**

617 **C2C12-derived muscle fibers to form neuromuscular junctions *in vitro***

618 (A) Representative bright-field images of the differentiated spinal motor neuron

spheroids based on differential co-culture medium compositions. Scale bar, 100 μm.

(B) Representative bright-field images of the differentiated muscle fibers based on differential co-culture medium compositions. Scale bar, 100 μm.

(C) Fold changes of mature motor neuron marker genes (NEUN, ChAT and VAChT) expression on differential co-culture medium. Data were collected from 2 independent experiments. Data are represented as mean ± SD.

(D) Fold changes of AChR markers (musk, chrng and chrne) genes expression on differential co-culture medium. Data were collected from 2 independent experiments. Data are represented as mean ± SD.

(E) Schematic illustration of co-culture model.

(F) Immunofluorescent images demonstrating motor neurons extending patterns when co-cultured with muscle fibers. Scale bar, 50 μm.

(G) Immunofluorescent staining of neuronal marker (TUJ1), mature muscle marker (MyHC) and AChR marker (α-BTX) on co-cultured cells. Scale bar, 50 μm.

Supplementary Figures titles and legends

Figure S1. Characterization of human NMPs and hSCNPCs from hPSCs

(A) Immunofluorescent staining of human NMP marker (CDX2) and the quantification results. Scale bar, 50 μm. n = 3 independent experiments. Data are represented as mean ± SD.

(B) Immunofluorescent staining of human NMP markers (SOX2 and Brachyury) of hiPSCs (DC60-3 and DC87-3)-derived NMPs and the quantification results. Scale bar, 50 μm. n = 3 independent experiments. Data are represented as mean ± SD.

(C) Immunofluorescent staining of human NMP marker (CDX2) of hiPSCs (DC60-3 and DC87-3)-derived NMPs and the quantification results. Scale bar, 50 μm. n = 3 independent experiments. Data are represented as mean ± SD.

(D) Relative marker genes expression of during NeuDet stage. n = 3 independent experiments. Data are represented as mean ± SD.

(E) Karyotyping of hSCNPCs at P40.

(F) Immunofluorescence analysis of hiPSCs (DC60-3 and DC87-3)-derived hiSCNPCs and the quantification results. Scale bar, 50 μm. n = 3 independent experiments. Data are represented as mean ± SD.

Figure S2. Characterization of hiSCNPCs and multi-potency of hSCNPCs

(A) Relative marker genes expression during spinal motor neuron differentiation from hSCNPCs. n = 3 independent experiments. Data are represented as mean ± SD.

(B) Immunostaining characterization of hiSCNPCs (Derived from hiPSCs lines DC60-3 and DC87-3) differentiated spinal motor neurons at day 18. Scale bar, 50 μm.

(C) The heat-map showing two regulon groups in samples of spinal motor neuron differentiation from hSCNPCs with listing representative regulon transcription factors (numbers of predicted target genes by SCENIC in the brackets) and enriched GO terms for each regulon group.

(D) Bright field of hSCNPCs spontaneous differentiated neurons. Scale bar, 500 μm.

(E) Immunofluorescent staining of hSCNPCs spontaneous differentiated neurons with neuronal marker TUJ1. Scale bar, 100 μm.

(F) Comparison of mir-218-2 expression levels during hSCNPCs spinal motor neuron differentiation and spontaneous differentiation. n = 2-3 independent experiments. Data are represented as mean ± SD.

(G) Immunostaining characterization of hSCNPCs with motor neuron marker (HB9), interneuron marker (GABA, SST) and astrocyte marker (S100β). Scale bar, 50 μm.

Figure S3. Electrophysiology of hSCNPCs differentiated spinal motor neurons.

(A) Bright field illustration of motor neuron under patch clamping. Scale bar, 50 μm.

(B) Immunofluorescent staining of TUJ1 and SMI-32 of spinal motor neurons co-culture with astrocyte at day 30. Scale bar, 50 μm.

(C) Sample AP traces in response to a series of step current injections from 0 pA to 60 pA.

(D) sPSCs of hSCNPCs are not observed in differentiated spinal motor neurons at day

30.

Figure S4. Generation of C2C12 myogenic differentiation.

(A) Schematic illustration of C2C12 SOP myogenic differentiation scheme.

(B) Immunofluorescent staining of mature muscle marker (MyHC) and acetylcholine receptor accumulation (α-BTX). Scale bar, 200 μm.

(C) Representative AChR images at C2C12 differentiated cell at day 6. Scale bar, 50 μm.

KEY RESOURCES TABLE

REAGENT or RESOURCE	SOURCE	IDENTIFIER
Antibodies		
Rabbit polyclonal antibody anti-SOX2	Abcam	Cat# ab97959, RRID: AB_2341193
Goat polyclonal antibody anti-Brachyury	R&D Systems	Cat# AF2085, RRID: AB_2200235
Mouse monoclonal antibody anti-Nestin	Millipore	Cat# MAB5326, RRID: AB_11211837
Goat polyclonal antibody anti-SOX1	R&D Systems	Cat# AF3369, RRID: AB_2239879
Mouse monoclonal antibody anti-PAX6	Abcam	Cat# ab78545, RRID: AB_1566562
Rabbit monoclonal antibody anti-Ki67	Abcam	Cat# ab16667, RRID:AB_302459
Mouse monoclonal antibody anti-NKX6-1	DSHB	Cat# F55A10, RRID:AB_532378
Mouse monoclonal antibody anti-NKX2-2	Novus Biologicals	Cat# NBP2-29432
Rabbit polyclonal antibody anti-Olig-2	Millipore	Cat# AB9610, RRID:AB_570666
Rabbit monoclonal antibody anti-CDX2	Abcam	Cat# ab76541, RRID:AB_1523334
Mouse monoclonal antibody anti-HB9	DSHB	Cat# 81.5C10, RRID:AB_2145209
Mouse monoclonal antibody anti-Islet-1	DSHB	Cat# 40.2D6, RRID:AB_528315
Mouse monoclonal antibody anti-Neurofilament H (SMI-32)	BioLegend	Cat# 801701, RRID:AB_2564642
Rabbit polyclonal antibody anti-NEUN	Millipore	Cat# ABN78, RRID:AB_10807945
Chicken polyclonal antibody anti-MAP2	BioLegend	Cat# 822501, RRID:AB_2564858
Goat polyclonal antibody anti-CHAT	Millipore	Cat# AB144P, RRID:AB_2079751
Rabbit polyclonal antibody anti-VAChT	Synaptic Systems	Cat# 139 103, RRID:AB_887864

Continued

REAGENT or RESOURCE	SOURCE	IDENTIFIER
Rabbit polyclonal antibody anti-VGLUT 1/2	Synaptic Systems	Cat# 135 503, RRID:AB_2285905
Mouse monoclonal antibody anti-GAD67	Millipore	Cat# MAB5406, RRID:AB_2278725
Rabbit polyclonal antibody anti-Tyrosine Hydroxylase	Millipore	Cat# AB152, RRID:AB_390204
Rat monoclonal antibody anti-HoxB4	DSHB	Cat# I12 anti-Hoxb4, RRID:AB_2119288
Rabbit polyclonal antibody anti-HoxC6	Abcam	Cat# ab41587, RRID:AB_942001
Mouse monoclonal antibody anti-HOXC9	Abcam	Cat# ab50839, RRID:AB_880494
Rabbit polyclonal antibody anti-HOXD10	Abcam	Cat# ab76897, RRID:AB_2041677
Rabbit polyclonal antibody anti-HOXD11	Proteintech	Cat# 18734-1-AP, RRID:AB_2878558
Rabbit monoclonal antibody anti-TUJ1	BioLegend	Cat# MRB-435P-100, RRID:AB_663339
Mouse monoclonal antibody anti-TUJ1	BioLegend	Cat# 801202, RRID:AB_10063408
Rabbit polyclonal antibody anti-GABA	Sigma-Aldrich	Cat# A2052, RRID:AB_477652
Rat monoclonal antibody anti-SST	Millipore	Cat# MAB354, RRID:AB_2255365
Rabbit polyclonal antibody anti-S100	Agilent	Cat# Z0311, RRID:AB_10013383
Rabbit monoclonal antibody anti-Synaptophysin	Abcam	Cat# ab32127, RRID:AB_2286949
Mouse monoclonal antibody anti-Synaptophysin 1	Synaptic Systems	Cat# 101 011, RRID:AB_887824
Rabbit polyclonal antibody anti-PSD95	Abcam	Cat# ab18258, RRID:AB_444362
Mouse monoclonal antibody anti-Myosin (Skeletal, Fast)	Sigma-Aldrich	Cat# M4276, RRID:AB_477190
α-Bungarotoxin, CF®594	Biotium	Cat# 00007
Chemicals, Peptides, and Recombinant Proteins		
bFGF	PeproTech	Car# 100-18B
CHIR-99021	Selleck	Car# S1263
SB431542	Selleck	Car# S1067

Continued

REAGENT or RESOURCE	SOURCE	IDENTIFIER
Dorsomorphin	Selleck	Car# S7840
Y27632	Selleck	Car# S1049
Compound E	Sigma-Aldrich	Car# 565790
Purmorphamine	Selleck	Car# S3042
FGF-8	R&D Systems	Cat# 423-F8-025
BDNF	PeproTech	Cat# 450-02
GDNF	PeproTech	Cat# 450-10
NT-3	PeproTech	Cat# 450-03
DMEM, High glucose	GIBCO	Cat# 11965092
DMEM/F-12, HEPES	GIBCO	Cat# 11330057
Neurobasal Medium	GIBCO	Cat# 21103049
NEAA	GIBCO	Cat# 11140050
GlutaMAX	GIBCO	Cat# 35050061
b-Mercaptoethanol	Sigma-Aldrich	Cat# M3148
Matrigel	Corning	Cat# 354277
Matrigel	Corning	Cat# 354230
Penicillin/streptomycin	GIBCO	Cat# 15140122
Accutase	GIBCO	Cat# A1110501
Poly-D-Lysine	GIBCO	Cat# A3890401
NeuroCult™ SM1	STEMCELL	Cat# 05731
N2 Supplement-A	STEMCELL	Cat# 07152
Laminin	GIBCO	Cat# 23017015
Terg-a-zyme	Sigma-Aldrich	Cat# Z273287
Trypsin (2.5%)	GIBCO	Cat# 15090046
Critical Commercial Assays		
FastQuant RT Kit (With gDNase)	TIANGEN	Cat# KR106
Stormstar SYBR Green qPCR MasterMix	DBI Bioscience	Cat# DBI-2143
Deposited Data		
RNA-Seq data	This paper	GSE
Experimental models: Cell lines		
H9 human embryonic stem cell line	WiCell Research Institute	Cat# SCSP-302

Continued

REAGENT or RESOURCE	SOURCE	IDENTIFIER
Human induced pluripotent stem cell line: DC60, clone 3	(Tao et al., 2020)	DC60-3
Human induced pluripotent stem cell line: DC87, clone 3	(Tao et al., 2020)	DC87-3
Oligonucleotides		
qPCR Primers	Table S1	N/A
Software and Algorithms		
ImageJ	ImageJ	https://imagej.nih.gov/ij/download.html
pCLAMP version 10.6	Molecular Devices	https://www.moleculardevices.com/products/axon-patch-clamp-system/acquisition-and-analysis-software/pclamp-software-suite
Graphpad Prism 6	GraphPad Software	https://www.graphpad.com/scientific-software/prism/
Fastp (v0.12.1)	(Chen et al., 2018)	https://github.com/OpenGene/fastp
Hisat2 (v2.1.0)	(Kim et al., 2015)	http://daehwankimlab.github.io/hisat2/
FeatureCounts (v1.5.3)	(Liao et al., 2014)	http://subread.sourceforge.net/featureCounts.html
ComBat	(Johnson et al., 2007)	https://rdrr.io/bioc/sva/src/R/ComBat.R
Principal Components Analysis (PCA)	(Jolliffe, 2002)	
scuttle	McCarthy et al., 2017	https://bioconductor.org/packages/release/bioc/html/scuttle.html
SCENIC	Aibar et al., 2017	https://scenic.aertslab.org/
Metascape	Zhou et al., 2019	https://metascape.org/

STAR★METHODS

LEAD CONTACT AND MATERIALS AVAILABILITY

For further information and requests for reagents and resource, please contact the leading correspondence Naihe Jing (njing@sibcb.ac.cn). All materials and reagents will be made available upon installment of a material transfer agreement (MTA).

hPSCs Culture

Human embryonic stem cells (H9) (Thomson et al., 1998) was obtained from WiCell Research Institute. Human induced pluripotent stem cells (DC60-3, DC87-3) were generated from human peripheral blood mononuclear cells (PBMNC) in our lab previously (Tao et al., 2020). Undifferentiated hPSCs were cultured in mTeSR1^{TM} medium (STEMCELL Technologies) on Matrigel (Corning, hESCs-qualified)-coated cell culture plates. mTeSR1^{TM} medium was changed every day and hPSCs clones were disassociated into small clumps with ReLeSR (STEMCELL Technologies) as required and passaged every 3-4 days.

Generation of human neuromesodermal progenitors from hPSCs

hPSCs (H9, DC60-3 and DC87-3) were disassociated into single cells with Accutase (Gibco) for 6-10 min at 37 ℃ incubator. hPSCs single cell suspension were counted and plated at a density of 45,000 cells/cm^2 in mTeSR1^{TM} medium on Matrigel (Corning)-coated cell culture plates for 1 day then cell culture medium was changed into hNMP differentiation medium at the second day and culture medium was changed every day up to day 4. 100 ml of hNMP differentiation medium composited with 47.5 ml of DMEM/F12 (Gibco), 47.5 ml of Neurobasal (Gibco), 1 ml of N2 (STEMCELL Technologies, 100X), 2 ml of NeuroCult™ SM1 Without Vitamin A (STEMCELL Technology, 50X), 1 ml of NEAA (Gibco), 1 ml of GlutaMAX (Gibco), 20 ng/ml FGF-2 (PeproTech), 3 μM CHIR99021 (Selleck), 10 μM SB431542 (Selleck), 20 μM Dorsomorphin (Selleck).

Generation of human spinal cord neural progenitor cells from hNMPs

hNMPs were disassociated into single cells with Accutase (Gibco), and plated at a density of 100,000 cells/cm^2 in hSCNPCs induction medium on Matrigel-coated cell culture plates. hSCNPCs induction medium was changed every day up to day 6. 100 ml of hSCNPCs induction medium composited with 47.5 ml of DMEM/F12 (Gibco), 47.5 ml of Neurobasal (Gibco), 1 ml of N2 (STEMCELL Technologies, 100X), 2 ml of NeuroCult™ SM1 Without Vitamin A (STEMCELL Technology, 50X), 1 ml of NEAA (Gibco), 1 ml of GlutaMAX (Gibco), 100 ng/ml FGF-2 (PeproTech), 100 ng/ml FGF-8 (PeproTech), 4 μM CHIR99021 (Selleck), 10 μM SB431542 (Selleck), 20 μM Dorsomorphin (Selleck), 0.2 μM Compound E (Sigma-Aldrich).

hSCNPCs culture

hSCNPCs were cultured in N2B27 medium supplemented with 2 μM SB431542, 3 μM CHIR99021, 0.25 μM Purmorphamine, 1X NEAA (Gibco), 1X GlutaMAX (Gibco) and 0.1 mM 2-Mercaptoethanol (Sigma-Aldrich), on Matrigel (Corning)-coated cell culture plates. hSCNPCs were dissociated into single cells with Accutase (Gibco), and were plated on Matrigel (Corning)-coated plates in a density of 300,000/cm^2 in hSCNPCs maintenance medium.

Spinal motor neuron differentiation from hSCNPCs

To differentiate hSCNPCs into motor neurons, hSCNPCs were dissociated into single cells with Accutase, counted and plated at a density of 100,000/cm^2 on pre-treated dish (Dish pre-treated with PDL coated for 2 hours, wash 3 times with sterilized water and then Matrigel coated for 2 hours). 100 ml of motor neuron differentiation medium composited with 47.5 ml of DMEM/F12 (Gibco), 47.5 ml of Neurobasal (Gibco), 1 ml of N2 (STEMCELL Technologies, 100X), 2 ml of NeuroCult™ SM1 Without Vitamin A (STEMCELL Technology, 50X), 1 ml of NEAA (Gibco), 1 ml of GlutaMAX (Gibco), 1 μM Purmorphamine, 0.2 μM Compound E, 10 ng/ml BDNF, 10 ng/ml GDNF, 10 ng/ml NT-3. 10 μM Y27632 was added at the plating day. The motor neuron differentiation medium was changed every other day.

Spontaneous differentiation of hSCNPCs

hSCNPCs were dissociated into single cells with Accutase (Gibco), and were plated at a density of 100,000/cm^2 on pre-treated dish (Dishes were pre-treated with PDL for 2 hours, washed 3 times with sterilized water and then re-coated with Matrigel for 2 hours). 100 ml of spontaneous differentiation medium composited with 47.5 ml of DMEM/F12 (Gibco), 47.5 ml of Neurobasal (Gibco), 1 ml of N2 (STEMCELL Technologies, 100X), 2 ml of NeuroCult™ SM1 Without Vitamin A (STEMCELL Technology, 50X), 1 ml of NEAA (Gibco), 1 ml of GlutaMAX (Gibco). 10 μM Y27632 was added at the plating day. The spontaneous differentiation medium was changed every other day.

3D spinal motor neuron spheroids differentiation from hSCNPCs

To generate 3D spinal motor neuron spheroids, hSCNPCs were digested into single cells with Accutase (Gibco), counted and distributed into V-bottom 96-well plate at a density of 50,000/well. 3D spinal motor neuron spheroids were differentiated in N2B27 medium contains Purmorphamine, Compound E, BDNF, GDNF, NT-3 and CultureOne^{TM} supplement (Gibco). Differentiation medium was changed every other day.

C2C12 maintenance and differentiation

C2C12 myoblasts were cultured in high-glucose DMEM medium with 10% FBS. The medium was changed every other day. To differentiate C2C12 into muscle fibers, C2C12 were dissociated into single cells with 0.05% trypsin, counted and plated in 45,000 cells/cm^2 on pre-coated dishes (Dishes were pre-treated with PDL for 2 hours, washed 3 times with sterilized water and then re-coated with Laminin for 2 hours) in C2C12 maintenance medium. On the following day, the C2C12 maintenance medium was replaced with differentiation medium (DMEM with 2% horse serum). Then the differentiation medium was changed every other day.

Co-culture of spinal motor neuron spheroids and C2C12-derived muscle fibers

To co-culture spinal motor neurons spheroids with C2C12-derived muscle fibers, we pre-differentiated C2C12 as described above, after two days of C2C12 differentiation, spinal motor neuron spheroids pre-differentiated for 12 days were plated onto C2C12-derived muscle fibers in co-culture medium (DMEM supplemented with 0.4% Ultroser^{TM} G and 10 ng/ml BDNF and 10 ng/ml GDNF and 10 µg/ml insulin. The co-culture medium was changed every other day.

Electrophysiology of spinal motor neurons

Whole-cell patch-clamp recordings were performed as previously described (Zhang et al., 2020). hPSCs-derived spinal motor neurons were cultured in a 35 mm petri dish. For recording, the neurons were perfused with the ACSF solution (in mM): 126 NaCl, 4.9 KCl, 1.2 KH_2PO_4, 2.4 $MgSO_4$, 2.5 $CaCl_2$, 26 $NaHCO_3$, 20 Glucose. Recording pipettes (8-10 MΩ) were fabricated using a P1000 micropipette puller (Sutter Instrument, USA) and filled with internal solution consisting of (in mM): 136 K-gluconate, 6 KCl, 1 EGTA, 2.5 Na_2ATP, 10 HEPES. For recording action potentials, cells were recorded at a holding potential of -70 mV and a series of step depolarizing currents were injected into cells in a current-clamp mode. All the recordings were performed using an Olympus microscope (BX51WI). The data were sampled at 10 Hz and collected with a low-pass filter at 2 kHz and analyzed using the Axopatch1500B amplifier and pCLAMP10 software (Molecular Devices) and GraphPad Prism 8.0.2.

HD-MEA recordings and analysis of hSCNPCs-derived spinal motor neurons

To analyze the function of hSCNPCs-derived motor neurons, we used high-content multi-electrode array system (MaxOne System, MaxWell Biosystems AG, Switzerland). MaxOne chips were pre-coated with 1% Terg-a-zyme (Sigma) overnight at room temperature and washed 3 times with sterile ddH_2O, then transfered MaxOne Chips in a beaker filled with 75% ethanol for 1 hour in a biological safety cabinet, and then washed 3 times with sterile ddH_2O, then 500 µl PDL was added for coating MaxOne chips for 2 hours at 37 ℃, then washed 3 times with sterile ddH_2O and re-coated

MaxOne chips with Matrigel (Corning) for 2 hours at 37 °C. hSCNPCs were dissociated into single cells, counted and plated on MaxOne chips at a density of 300,000 cells/chip in motor neuron differentiation medium. MEA data recording started after 6 days of plating and measured every 6 days till day 42.

For MEA data recording, MaxLab Live Software (v.21.1.2. MaxWell Biosystems AG, Switzerland) was used. Assays were chosen from assay gallery which contains three assays, activity scan, network and axon recording. To be able to track axons, we first recorded the whole MaxOne HD-MEA surface using the "Activity Scan Assay" module, featured in the MaxLab Live software (MaxWell Biosystems AG, Zurich, Switzerland). 29 electrode configurations, including a total of 26,400 electrodes at a distance of 17.5 µm, were used to record the spontaneous neuronal electrical activity across the entire MaxOne HD-MEA. Each electrode configuration was recorded for 60 seconds.

In a next step, axonal signals were identified with the "Axon Tracking Assay" module of the MaxLab Live software, which uses a tailored recording strategy similar to the ones described in previous publications (Bakkum et al., 2013; Bullmann et al., 2019; Radivojevic et al., 2017). First, a set of 30 target neurons was identified by selecting the positions of 30 electrodes featuring the largest spike amplitude, keeping a minimum distance of 17.5 µm between each two target neurons. For every target neuron, a 3×3 electrodes block (distance between electrodes 17.5 µm) was selected around the central electrode. After defining the 3×3 blocks, a set of sequential 180 s recordings that covered larger array areas (300×300 to 800×800 μm^2 around the blocks) was run, where the 3×3 central blocks were always included in every recording.

The detected spikes on the 3×3 electrode blocks were then sorted using a K-Means clustering algorithm (Lewicki, 1998) based on the action potential minimum spike amplitude. Spike sorting results were used to reconstruct the spike-triggered average extracellular waveform over the recorded array area for every identified neuron. An unsupervised object-tracking algorithm was then used to detect the path of action potential signal propagation, thus identifying (1) individual axonal branches and (2) the morphology of neuronal outgrowth per cell. The axonal conduction velocity was then calculated for every detected axonal branch.

Immunocytochemistry

Cells were fixed with 4% paraformaldehyde (PFA, Sigma-Aldrich) for 20 minutes at room temperature then washed 3 times with PBS. Blocking with 0.3% Triton X-100 /5% fetal bovine serum in PBS for one hour at room temperature. Primary antibodies were diluted in 0.3% Triton X-100 /5% fetal bovine serum in PBS and incubated overnight at 4 ℃. Samples were washed in PBS for three times and then incubated with secondary antibodies (1:200-1:1000) in 0.3% Triton X-100 /5% fetal bovine serum in PBS for two hours. Images were taken with Leica TCS SP8 confocal laser-scanning microscope.

RT-qPCR analysis

Total RNA was extracted from cultured cells by using the TRIzol reagent, and cDNA was reverse-transcribed, starting from 1000 ng of total RNA with the SuperScript III First-strand cDNA synthesis kit (Invitrogen). qPCR was performed using Mastercycler RealPlex2 (Eppendorf) and Stormstar SYBR Green qPCR MasterMix (DBI Bioscience). Data were normalized for GAPDH expression. The primers sequences used for qPCR amplification were listed in Table S1.

RNA-Sequencing and data analysis

Cell samples at different stages were collected and mRNA-seq libraries were constructed with NEBNext® Ultra™ II Library Prep Kit for Illumina. Qualified libraries were multiplexed and sequenced on Illumina NovaSeq 6000 according to the manufacturer's instructions (Illumina, USA). The Sequencing mode was PE150.

For data analysis, reference genome and gene annotation files were downloaded from GENECODE (hg38). Fastq files were pre-processed by Fastp (v0.12.1) (Chen et al., 2018) with default parameters. Cleaned data were then aligned to the reference genome via Hisat2 (v2.1.0) (Kim et al., 2015). FeatureCounts (v1.5.3) (Liao et al., 2014) was used to count the reads mapped to each gene.

Correlation to nmps

RNA-seq data in this paper were compared with nmps (Verrier et al., 2018) after removing batch effects by the R package "ComBat" (Johnson et al., 2007). Principal Components Analysis (PCA) (Jolliffe, 2002) was used to show the correlation of these samples.

Correlation to BRAINSPAN database and pseudo-bulk RNA-seq of human single cell spinal cord

The 'Developmental Transcriptome Dataset' of BRAINSPAN (https://www.brainspan.org/static/download.html) was also downloaded. We merged the brain samples of same stage and calculated Pearson correlation coefficients between the merged samples and RNA-seq data in this paper.

Pseudo-bulk RNA-seq of human spinal cord, GSE171892 (Rayon et al., 2021), was conducted through the R package "scuttle" (McCarthy et al., 2017). After that, samples at same stages were merged and Pearson correlation coefficients were calculated between the pseudo-bulk RNA-seq and RNA-seq data in this paper.

Inference of regulons and their activity

The SCENIC (Aibar et al., 2017) was used to infer the gene regulatory network (regulon). Binary regulon-activity matrix for all samples was used in principal components analysis. GO enrichment analysis of related target genes was carried out by Metascape (https://metascape.org/) with default parameters (Zhou et al., 2019).

Statistical analysis

All statistical analyses were performed in GraphPad Prism software (GraphPad Prism 8.0.2). Cell counting, RT-qPCR data and electrophysiological data were presented as mean ± SD. Student's t test (two-tailed) was performed for statistical analysis between two groups. Sample size (n) values were provided in the relevant text, figures, and figure legends. The statistical analyses were obtained from three independent experiments. Statistical significance was set at p values.

Data availability

All RNA-seq data are available at the Gene Expression Omnibus (GEO) under accession number GSE205718.

REFERENCES

Aibar, S., González-Blas, C.B., Moerman, T., Huynh-Thu, V.A., Imrichova, H., Hulselmans, G., Rambow, F., Marine, J.C., Geurts, P., Aerts, J., et al. (2017). SCENIC: single-cell regulatory network inference and clustering. Nat Methods 14, 1083-1086.

Amin, N.D., Bai, G., Klug, J.R., Bonanomi, D., Pankratz, M.T., Gifford, W.D., Hinckley, C.A., Sternfeld, M.J., Driscoll, S.P., and Dominguez, B.J.S. (2015). Loss of motoneuron-specific microRNA-218 causes systemic neuromuscular failure. 350, 1525-1529.

Amin, N.D., Senturk, G., Costaguta, G., Driscoll, S., O'Leary, B., Bonanomi, D., and Pfaff, S.L. (2021). A hidden threshold in motor neuron gene networks revealed by modulation of miR-218 dose. Neuron 109, 3252-3267 e3256.

Bakkum, D.J., Frey, U., Radivojevic, M., Russell, T.L., Muller, J., Fiscella, M., Takahashi, H., and Hierlemann, A. (2013). Tracking axonal action potential propagation on a high-density microelectrode array across hundreds of sites. Nat Commun 4, 2181.

Bakooshli, M.A., Lippmann, E.S., Mulcahy, B., Iyer, N., Nguyen, C.T., Tung, K., Stewart, B.A., van den Dorpel, H., Fuehrmann, T., and Shoichet, M.J.E. (2019). A 3D culture model of innervated human skeletal muscle enables studies of the adult neuromuscular junction. 8, e44530.

Barbeau, S., Tahraoui-Bories, J., Legay, C., and Martinat, C.J.D. (2020). Building neuromuscular junctions in vitro. 147, dev193920.

Ben-Shushan, E., Feldman, E., and Reubinoff, B.E. (2015). Notch signaling regulates motor neuron differentiation of human embryonic stem cells. Stem Cells 33, 403-415.

Bullmann, T., Radivojevic, M., Huber, S.T., Deligkaris, K., Hierlemann, A., and Frey, U. (2019). Large-Scale Mapping of Axonal Arbors Using High-Density Microelectrode Arrays. Front Cell Neurosci 13, 404.

954 Ceto, S., Sekiguchi, K.J., Takashima, Y., Nimmerjahn, A., and Tuszynski, M.H.J.C.s.c.
955 (2020). Neural stem cell grafts form extensive synaptic networks that integrate with
956 host circuits after spinal cord injury. 27, 430-440. e435.
957 Chambers, S.M., Fasano, C.A., Papapetrou, E.P., Tomishima, M., Sadelain, M., and
958 Studer, L. (2009). Highly efficient neural conversion of human ES and iPS cells by dual
959 inhibition of SMAD signaling. Nat Biotechnol 27, 275-280.
960 Chapman, D.L., and Papaioannou, V.E.J.N. (1998). Three neural tubes in mouse
961 embryos with mutations in the T-box gene Tbx6. 391, 695-697.
962 Chen, S., Zhou, Y., Chen, Y., and Gu, J. (2018). fastp: an ultra-fast all-in-one FASTQ
963 preprocessor. Bioinformatics (Oxford, England) 34, i884-i890.
964 Clowry, G., Sieradzan, K., and Vrbová, G.J.T.i.n. (1991). Transplants of embryonic
965 motoneurones to adult spinal cord: survival and innervation abilities. 14, 355-357.
966 Cutarelli, A., Martinez-Rojas, V.A., Tata, A., Battistella, I., Rossi, D., Arosio, D., Musio,
967 C., and Conti, L. (2021). A Monolayer System for the Efficient Generation of Motor
968 Neuron Progenitors and Functional Motor Neurons from Human Pluripotent Stem Cells.
969 Cells 10.
970 Dasen, J.S., Tice, B.C., Brenner-Morton, S., and Jessell, T.M. (2005). A Hox regulatory
971 network establishes motor neuron pool identity and target-muscle connectivity. Cell
972 123, 477-491.
973 Davis-Dusenbery, B.N., Williams, L.A., Klim, J.R., and Eggan, K. (2014). How to
974 make spinal motor neurons. Development 141, 491-501.
975 De Marco Garcia, N.V., and Jessell, T.M. (2008). Early motor neuron pool identity and
976 muscle nerve trajectory defined by postmitotic restrictions in Nkx6.1 activity. Neuron
977 57, 217-231.
978 Du, Z.W., Chen, H., Liu, H., Lu, J., Qian, K., Huang, C.L., Zhong, X., Fan, F., and
979 Zhang, S.C. (2015). Generation and expansion of highly pure motor neuron progenitors
980 from human pluripotent stem cells. Nat Commun 6, 6626.
981 Ebert, A.D., and Svendsen, C.N.J.N.R.D.D. (2010). Human stem cells and drug
982 screening: opportunities and challenges. 9, 367-372.
983 Fujimori, K., Ishikawa, M., Otomo, A., Atsuta, N., Nakamura, R., Akiyama, T., Hadano,

S., Aoki, M., Saya, H., Sobue, G., et al. (2018). Modeling sporadic ALS in iPSC-derived motor neurons identifies a potential therapeutic agent. Nat Med 24, 1579-1589.

Gouti, M., Tsakiridis, A., Wymeersch, F.J., Huang, Y., Kleinjung, J., Wilson, V., and Briscoe, J. (2014). In vitro generation of neuromesodermal progenitors reveals distinct roles for wnt signalling in the specification of spinal cord and paraxial mesoderm identity. PLoS Biol 12, e1001937.

Guo, X., Gonzalez, M., Stancescu, M., Vandenburgh, H.H., and Hickman, J.J. (2011). Neuromuscular junction formation between human stem cell-derived motoneurons and human skeletal muscle in a defined system. Biomaterials 32, 9602-9611.

Guthrie, S. (2004). Neuronal Development: Putting Motor Neurons in Their Place. Current Biology 14, R166-R168.

Henrique, D., Abranches, E., Verrier, L., and Storey, K.G. (2015). Neuromesodermal progenitors and the making of the spinal cord. Development 142, 2864-2875.

Hester, M.E., Murtha, M.J., Song, S., Rao, M., Miranda, C.J., Meyer, K., Tian, J., Boulting, G., Schaffer, D.V., Zhu, M.X., et al. (2011). Rapid and efficient generation of functional motor neurons from human pluripotent stem cells using gene delivered transcription factor codes. Mol Ther 19, 1905-1912.

Hoye, M.L., Regan, M.R., Jensen, L.A., Lake, A.M., Reddy, L.V., Vidensky, S., Richard, J.P., Maragakis, N.J., Rothstein, J.D., Dougherty, J.D., et al. (2018). Motor neuron-derived microRNAs cause astrocyte dysfunction in amyotrophic lateral sclerosis. Brain 141, 2561-2575.

Hu, B.Y., and Zhang, S.C. (2009). Differentiation of spinal motor neurons from pluripotent human stem cells. Nat Protoc 4, 1295-1304.

Hudish, L.I., Bubak, A., Triolo, T.M., Niemeyer, C.S., Lorberbaum, D.S., Sussel, L., Nagel, M., Taliaferro, J.M., and Russ, H.A. (2020). Modeling Hypoxia-Induced Neuropathies Using a Fast and Scalable Human Motor Neuron Differentiation System. Stem Cell Reports 14, 1033-1043.

Johnson, W.E., Li, C., and Rabinovic, A. (2007). Adjusting batch effects in microarray expression data using empirical Bayes methods. Biostatistics (Oxford, England) 8, 118-127.

1014 Jolliffe, I.T. (2002). Principal component analysis for special types of data (Springer).
1015 Kadoya, K., Lu, P., Nguyen, K., Lee-Kubli, C., Kumamaru, H., Yao, L., Knackert, J.,
1016 Poplawski, G., Dulin, J.N., Strobl, H., et al. (2016). Spinal cord reconstitution with
1017 homologous neural grafts enables robust corticospinal regeneration. Nat Med 22, 479-
1018 487.
1019 Kanning, K.C., Kaplan, A., and Henderson, C.E.J.A.r.o.n. (2010). Motor neuron
1020 diversity in development and disease. 33, 409-440.
1021 Karagiannis, P., Takahashi, K., Saito, M., Yoshida, Y., Okita, K., Watanabe, A., Inoue,
1022 H., Yamashita, J.K., Todani, M., and Nakagawa, M.J.P.r. (2019). Induced pluripotent
1023 stem cells and their use in human models of disease and development. 99, 79-114.
1024 Kariya, S., Obis, T., Garone, C., Akay, T., Sera, F., Iwata, S., Homma, S., and Monani,
1025 U.R. (2014). Requirement of enhanced Survival Motoneuron protein imposed during
1026 neuromuscular junction maturation. J Clin Invest 124, 785-800.
1027 Kim, D., Langmead, B., and Salzberg, S.L. (2015). HISAT: a fast spliced aligner with
1028 low memory requirements. Nat Methods 12, 357-360.
1029 Kumamaru, H., Kadoya, K., Adler, A.F., Takashima, Y., Graham, L., Coppola, G., and
1030 Tuszynski, M.H. (2018). Generation and post-injury integration of human spinal cord
1031 neural stem cells. Nat Methods 15, 723-731.
1032 Kumamaru, H., Lu, P., Rosenzweig, E.S., Kadoya, K., and Tuszynski, M.H.J.C.r. (2019).
1033 Regenerating corticospinal axons innervate phenotypically appropriate neurons within
1034 neural stem cell grafts. 26, 2329-2339. e2324.
1035 Lee, H., Shamy, G.A., Elkabetz, Y., Schofield, C.M., Harrsion, N.L., Panagiotakos, G.,
1036 Socci, N.D., Tabar, V., and Studer, L. (2007). Directed differentiation and
1037 transplantation of human embryonic stem cell-derived motoneurons. Stem Cells 25,
1038 1931-1939.
1039 Lewicki, M.S.J.N.C.i.N.S. (1998). A review of methods for spike sorting: the detection
1040 and classification of neural action potentials. 9, R53.
1041 Li, X.J., Du, Z.W., Zarnowska, E.D., Pankratz, M., Hansen, L.O., Pearce, R.A., and
1042 Zhang, S.C. (2005). Specification of motoneurons from human embryonic stem cells.
1043 Nat Biotechnol 23, 215-221.

1044 Li, X.J., Hu, B.Y., Jones, S.A., Zhang, Y.S., Lavaute, T., Du, Z.W., and Zhang, S.C.
1045 (2008). Directed differentiation of ventral spinal progenitors and motor neurons from
1046 human embryonic stem cells by small molecules. Stem Cells 26, 886-893.
1047 Liao, Y., Smyth, G.K., and Shi, W. (2014). featureCounts: an efficient general purpose
1048 program for assigning sequence reads to genomic features. Bioinformatics (Oxford,
1049 England) 30, 923-930.
1050 Lu, C.C., Brennan, J., Robertson, E.J.J.C.o.i.g., and development (2001). From
1051 fertilization to gastrulation: axis formation in the mouse embryo. 11, 384-392.
1052 Mahony, S., Mazzoni, E.O., McCuine, S., Young, R.A., Wichterle, H., and Gifford,
1053 D.K.J.G.b. (2011). Ligand-dependent dynamics of retinoic acid receptor binding during
1054 early neurogenesis. 12, 1-15.
1055 Mangold, O.J.N. (1933). Über die Induktionsfähigkeit der verschiedenen Bezirke der
1056 Neurula von Urodelen. 21, 761-766.
1057 Martins, J.-M.F., Fischer, C., Urzi, A., Vidal, R., Kunz, S., Ruffault, P.-L., Kabuss, L.,
1058 Hube, I., Gazzerro, E., and Birchmeier, C.J.C.s.c. (2020). Self-organizing 3D human
1059 trunk neuromuscular organoids. 26, 172-186. e176.
1060 Mazzoni, E.O., Mahony, S., Peljto, M., Patel, T., Thornton, S.R., McCuine, S., Reeder,
1061 C., Boyer, L.A., Young, R.A., Gifford, D.K., et al. (2013). Saltatory remodeling of Hox
1062 chromatin in response to rostrocaudal patterning signals. Nat Neurosci 16, 1191-1198.
1063 McCarthy, D.J., Campbell, K.R., Lun, A.T., and Wills, Q.F. (2017). Scater: pre-
1064 processing, quality control, normalization and visualization of single-cell RNA-seq
1065 data in R. Bioinformatics (Oxford, England) 33, 1179-1186.
1066 Metzis, V., Steinhauser, S., Pakanavicius, E., Gouti, M., Stamataki, D., Ivanovitch, K.,
1067 Watson, T., Rayon, T., Mousavy Gharavy, S.N., Lovell-Badge, R., et al. (2018).
1068 Nervous System Regionalization Entails Axial Allocation before Neural Differentiation.
1069 Cell 175, 1105-1118 e1117.
1070 Muller, J., Ballini, M., Livi, P., Chen, Y., Radivojevic, M., Shadmani, A., Viswam, V.,
1071 Jones, I.L., Fiscella, M., Diggelmann, R., et al. (2015). High-resolution CMOS MEA
1072 platform to study neurons at subcellular, cellular, and network levels. Lab Chip 15,
1073 2767-2780.

Narasimhan, K.J.N.N. (2006). Quantifying motor neuron loss in ALS. 9, 304-304.

Nieuwkoop, P.D., and Nigtevecht, G.v. (1954). Neural activation and transformation in explants of competent ectoderm under the influence of fragments of anterior notochord in urodeles.

Nijssen, J., Comley, L.H., and Hedlund, E.J.A.n. (2017). Motor neuron vulnerability and resistance in amyotrophic lateral sclerosis. 133, 863-885.

Olmsted, Z.T., Stigliano, C., Scimemi, A., Wolfe, T., Cibelli, J., Horner, P.J., and Paluh, J.L. (2021). Transplantable human motor networks as a neuron-directed strategy for spinal cord injury. iScience 24, 102827.

Osaki, T., Uzel, S.G., and Kamm, R.D.J.N.p. (2020). On-chip 3D neuromuscular model for drug screening and precision medicine in neuromuscular disease. 15, 421-449.

Patani, R., Hollins, A.J., Wishart, T.M., Puddifoot, C.A., Alvarez, S., de Lera, A.R., Wyllie, D.J., Compston, D.A., Pedersen, R.A., Gillingwater, T.H., et al. (2011). Retinoid-independent motor neurogenesis from human embryonic stem cells reveals a medial columnar ground state. Nat Commun 2, 214.

Picchiarelli, G., Demestre, M., Zuko, A., Been, M., Higelin, J., Dieterle, S., Goy, M.A., Mallik, M., Sellier, C., Scekic-Zahirovic, J., et al. (2019). FUS-mediated regulation of acetylcholine receptor transcription at neuromuscular junctions is compromised in amyotrophic lateral sclerosis. Nat Neurosci 22, 1793-1805.

Qu, Q., Li, D., Louis, K.R., Li, X., Yang, H., Sun, Q., Crandall, S.R., Tsang, S., Zhou, J., Cox, C.L., et al. (2014). High-efficiency motor neuron differentiation from human pluripotent stem cells and the function of Islet-1. Nat Commun 5, 3449.

Radivojevic, M., Franke, F., Altermatt, M., Muller, J., Hierlemann, A., and Bakkum, D.J. (2017). Tracking individual action potentials throughout mammalian axonal arbors. Elife 6.

Rayon, T., Maizels, R.J., Barrington, C., and Briscoe, J. (2021). Single-cell transcriptome profiling of the human developing spinal cord reveals a conserved genetic programme with human-specific features. Development 148.

Reichenstein, I., Eitan, C., Diaz-Garcia, S., Haim, G., Magen, I., Siany, A., Hoye, M.L., Rivkin, N., Olender, T., and Toth, B.J.S.t.m. (2019). Human genetics and

1104 neuropathology suggest a link between miR-218 and amyotrophic lateral sclerosis
1105 pathophysiology. 11, eaav5264.
1106 Sances, S., Bruijn, L.I., Chandran, S., Eggan, K., Ho, R., Klim, J.R., Livesey, M.R.,
1107 Lowry, E., Macklis, J.D., Rushton, D., et al. (2016). Modeling ALS with motor neurons
1108 derived from human induced pluripotent stem cells. Nat Neurosci 19, 542-553.
1109 Sockanathan, S., and Jessell, T.M.J.C. (1998). Motor neuron–derived retinoid signaling
1110 specifies the subtype identity of spinal motor neurons. 94, 503-514.
1111 Solnica-Krezel, L. (2005). Conserved patterns of cell movements during vertebrate
1112 gastrulation. Curr Biol 15, R213-228.
1113 Son, E.Y., Ichida, J.K., Wainger, B.J., Toma, J.S., Rafuse, V.F., Woolf, C.J., and Eggan,
1114 K. (2011). Conversion of mouse and human fibroblasts into functional spinal motor
1115 neurons. Cell Stem Cell 9, 205-218.
1116 Stern, C.D.J.N.R.N. (2001). Initial patterning of the central nervous system: how many
1117 organizers? 2, 92-98.
1118 Storey, K.G., Crossley, J.M., De Robertis, E.M., Norris, W.E., and Stern, C.D.J.D.
1119 (1992). Neural induction and regionalisation in the chick embryo. 114, 729-741.
1120 Sundberg, M., Pinson, H., Smith, R.S., Winden, K.D., Venugopal, P., Tai, D.J.C.,
1121 Gusella, J.F., Talkowski, M.E., Walsh, C.A., Tegmark, M., et al. (2021). 16p11.2
1122 deletion is associated with hyperactivation of human iPSC-derived dopaminergic
1123 neuron networks and is rescued by RHOA inhibition in vitro. Nat Commun 12, 2897.
1124 Takahashi, K., Tanabe, K., Ohnuki, M., Narita, M., Ichisaka, T., Tomoda, K., and
1125 Yamanaka, S.J.c. (2007). Induction of pluripotent stem cells from adult human
1126 fibroblasts by defined factors. 131, 861-872.
1127 Tam, P.P., and Behringer, R.R.J.M.o.d. (1997). Mouse gastrulation: the formation of a
1128 mammalian body plan. 68, 3-25.
1129 Tao, R., Lu, R., Wang, J., Zeng, S., Zhang, T., Guo, W., Zhang, X., Cheng, Q., Yue, C.,
1130 Wang, Y., et al. (2020). Probing the therapeutic potential of TRPC6 for Alzheimer's
1131 disease in live neurons from patient-specific iPSCs. J Mol Cell Biol 12, 807-816.
1132 Thomson, J.A., Itskovitz-Eldor, J., Shapiro, S.S., Waknitz, M.A., Swiergiel, J.J.,
1133 Marshall, V.S., and Jones, J.M.J.s. (1998). Embryonic stem cell lines derived from

human blastocysts. 282, 1145-1147.

Turner, D.A., Hayward, P.C., Baillie-Johnson, P., Rue, P., Broome, R., Faunes, F., and Martinez Arias, A. (2014). Wnt/beta-catenin and FGF signalling direct the specification and maintenance of a neuromesodermal axial progenitor in ensembles of mouse embryonic stem cells. Development 141, 4243-4253.

Tzouanacou, E., Wegener, A., Wymeersch, F.J., Wilson, V., and Nicolas, J.F. (2009). Redefining the progression of lineage segregations during mammalian embryogenesis by clonal analysis. Dev Cell 17, 365-376.

Varadarajan, S.G., Hunyara, J.L., Hamilton, N.R., Kolodkin, A.L., and Huberman, A.D.J.C. (2022). Central nervous system regeneration. 185, 77-94.

Verrier, L., Davidson, L., Gierlinski, M., Dady, A., and Storey, K.G. (2018). Neural differentiation, selection and transcriptomic profiling of human neuromesodermal progenitor-like cells in vitro. Development 145.

Wang, Z.B., Zhang, X., and Li, X.J. (2013). Recapitulation of spinal motor neuron-specific disease phenotypes in a human cell model of spinal muscular atrophy. Cell Res 23, 378-393.

Wind, M., Gogolou, A., Manipur, I., Granata, I., Butler, L., Andrews, P.W., Barbaric, I., Ning, K., Guarracino, M.R., and Placzek, M.J.D. (2021). Defining the signalling determinants of a posterior ventral spinal cord identity in human neuromesodermal progenitor derivatives. 148, dev194415.

Yu, J., Vodyanik, M.A., Smuga-Otto, K., Antosiewicz-Bourget, J., Frane, J.L., Tian, S., Nie, J., Jonsdottir, G.A., Ruotti, V., and Stewart, R.J.s. (2007). Induced pluripotent stem cell lines derived from human somatic cells. 318, 1917-1920.

Yuan, X., Schroter, M., Obien, M.E.J., Fiscella, M., Gong, W., Kikuchi, T., Odawara, A., Noji, S., Suzuki, I., Takahashi, J., et al. (2020). Versatile live-cell activity analysis platform for characterization of neuronal dynamics at single-cell and network level. Nat Commun 11, 4854.

Zhang, K., Yu, F., Zhu, J., Han, S., Chen, J., Wu, X., Chen, Y., Shen, T., Liao, J., Guo, W., et al. (2020). Imbalance of Excitatory/Inhibitory Neuron Differentiation in Neurodevelopmental Disorders with an NR2F1 Point Mutation. Cell Rep 31, 107521.

1164 Zhang, T., Ke, W., Zhou, X., Qian, Y., Feng, S., Wang, R., Cui, G., Tao, R., Guo, W.,
1165 Duan, Y., et al. (2019). Human Neural Stem Cells Reinforce Hippocampal Synaptic
1166 Network and Rescue Cognitive Deficits in a Mouse Model of Alzheimer's Disease.
1167 Stem Cell Reports 13, 1022-1037.
1168 Zhou, Y., Zhou, B., Pache, L., Chang, M., Khodabakhshi, A.H., Tanaseichuk, O.,
1169 Benner, C., and Chanda, S.K. (2019). Metascape provides a biologist-oriented resource
1170 for the analysis of systems-level datasets. Nat Commun 10, 1523.
1171

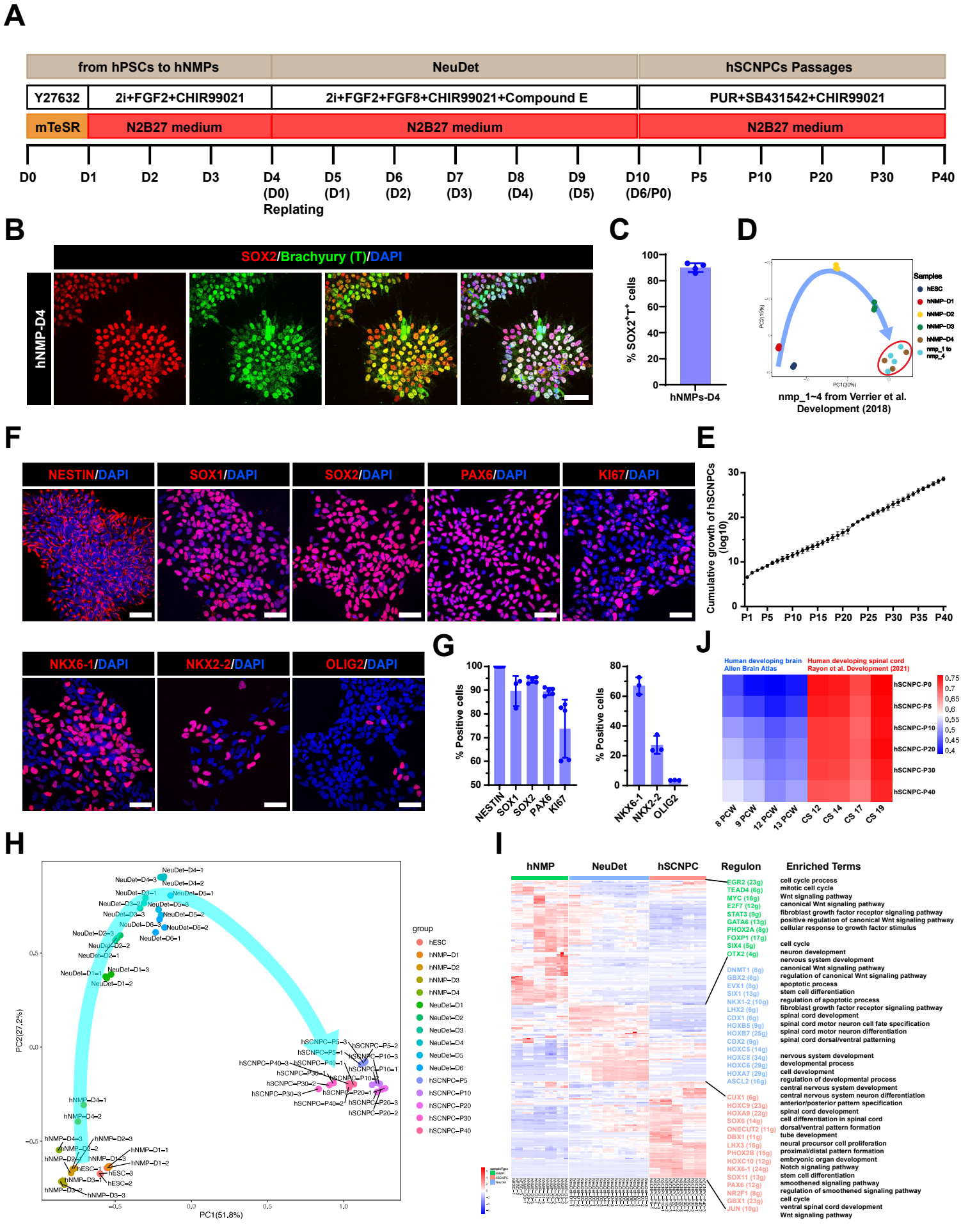

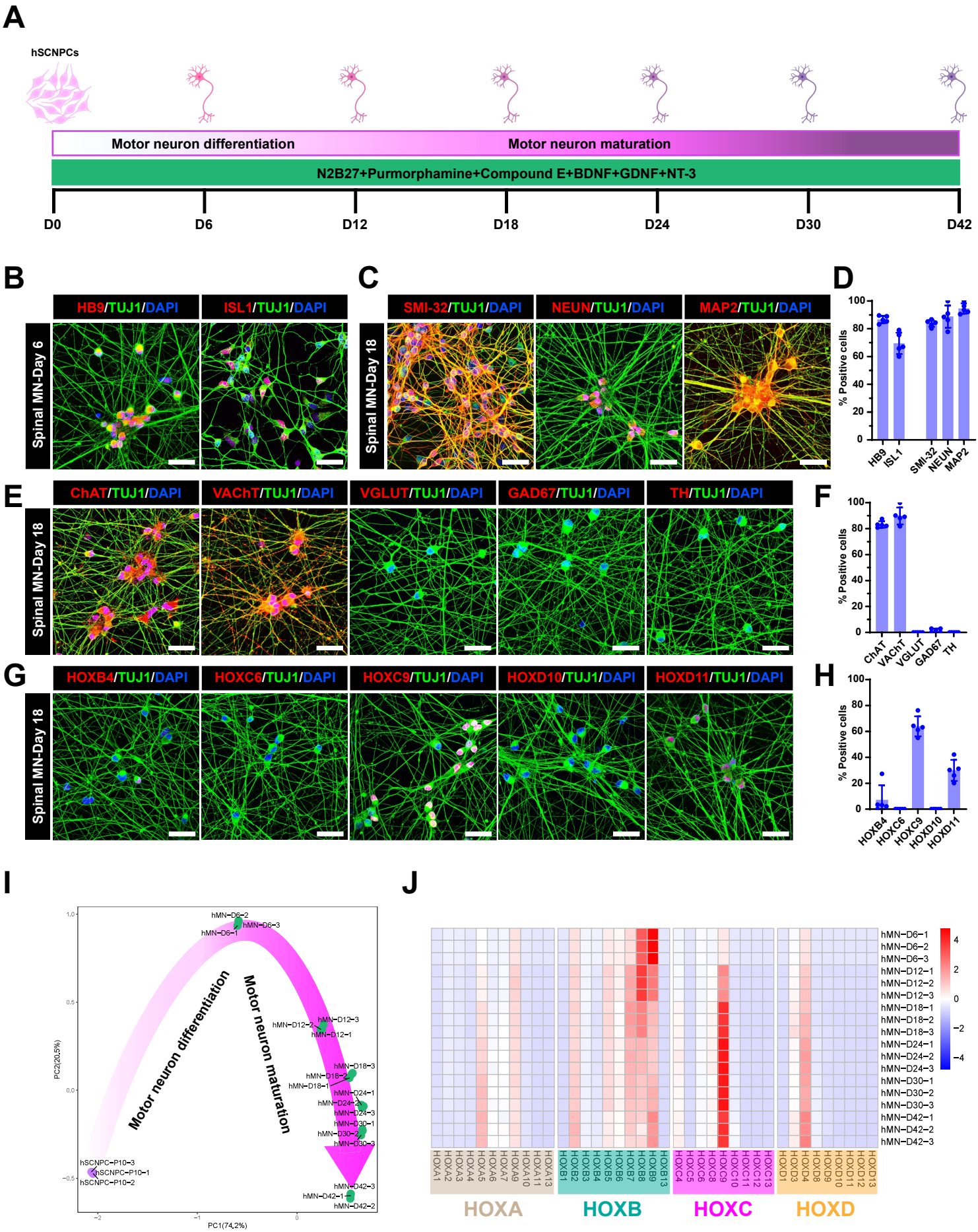

Xu et al., Figure 3

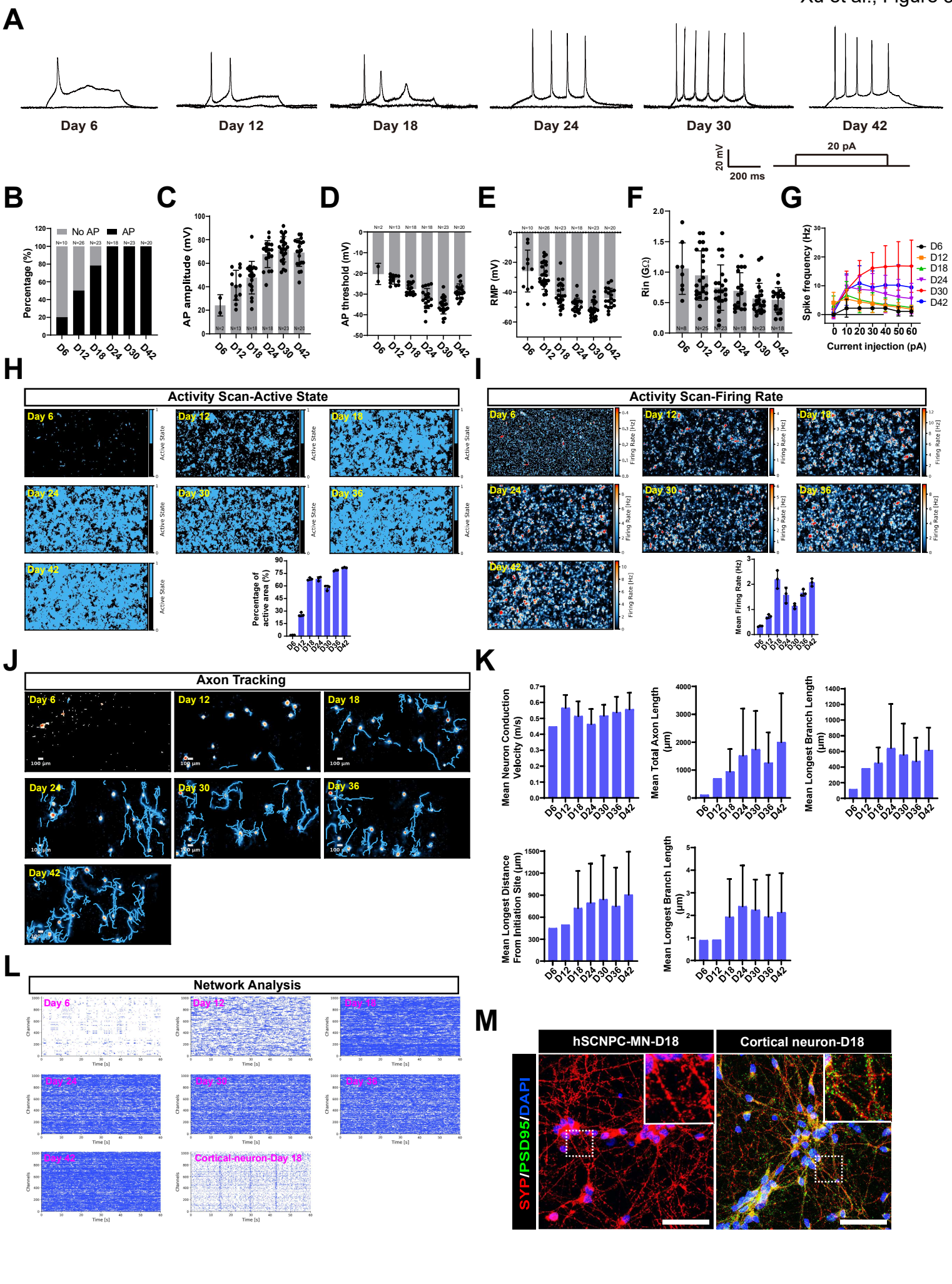

Xu et al., Figure 4

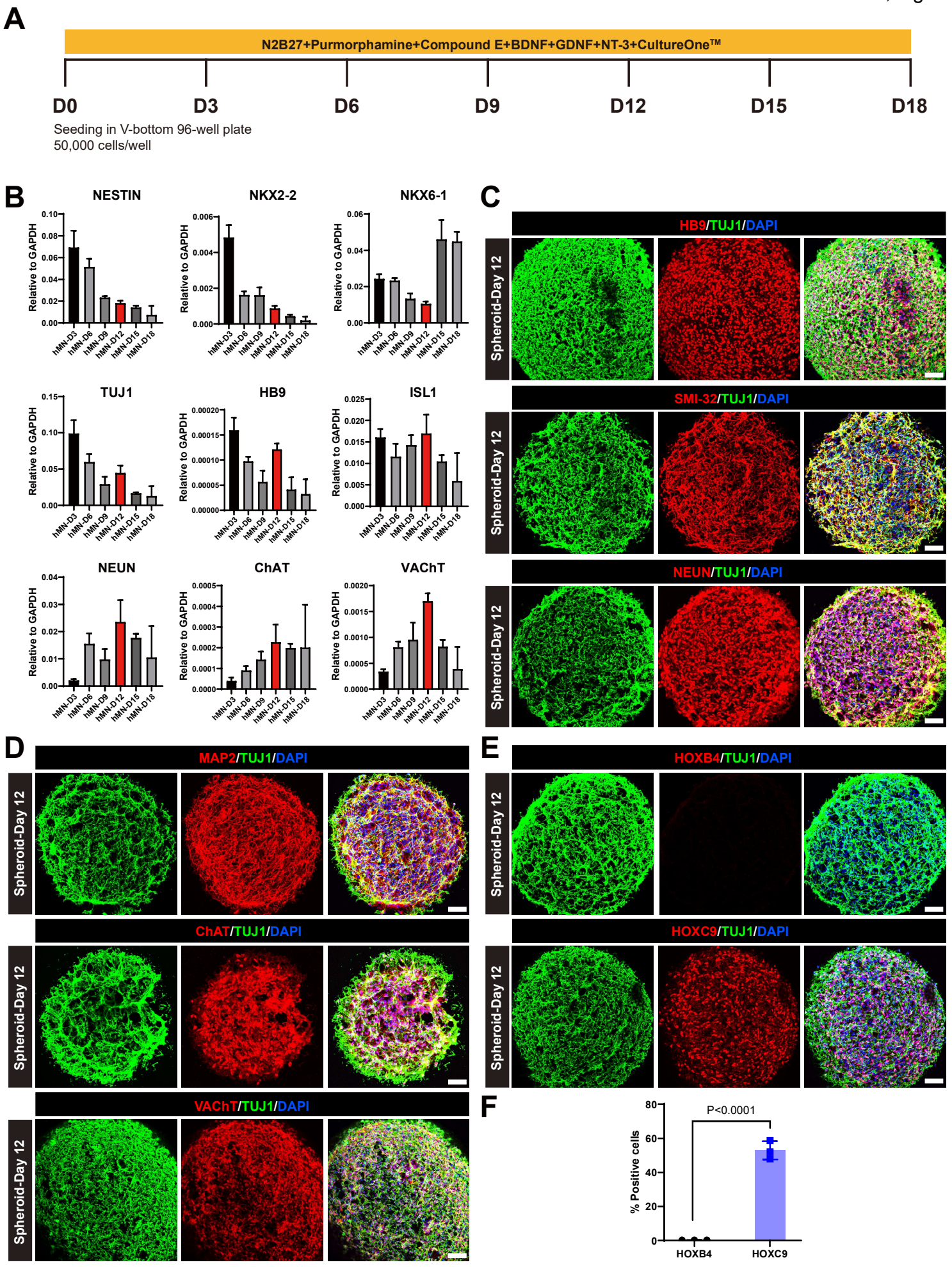

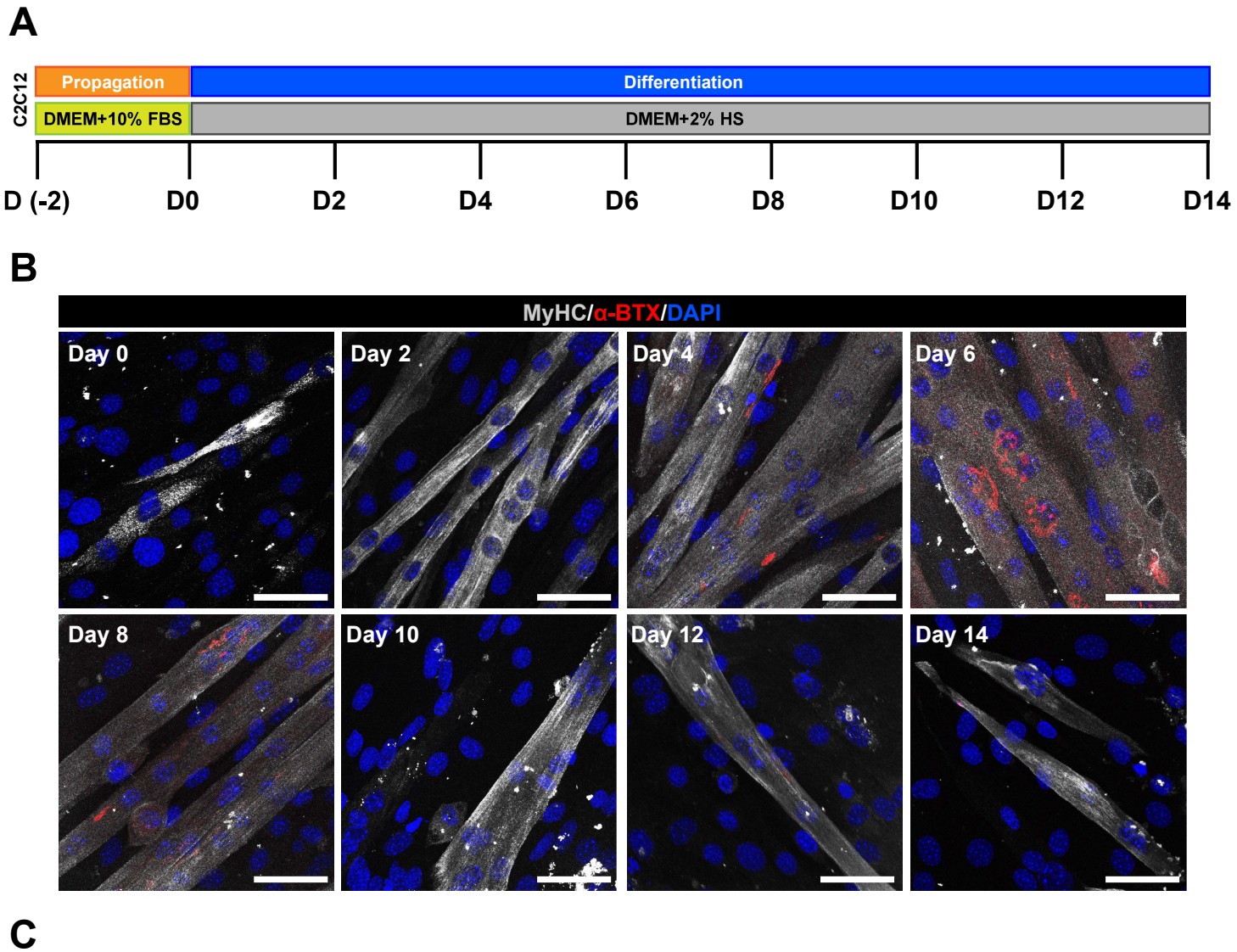

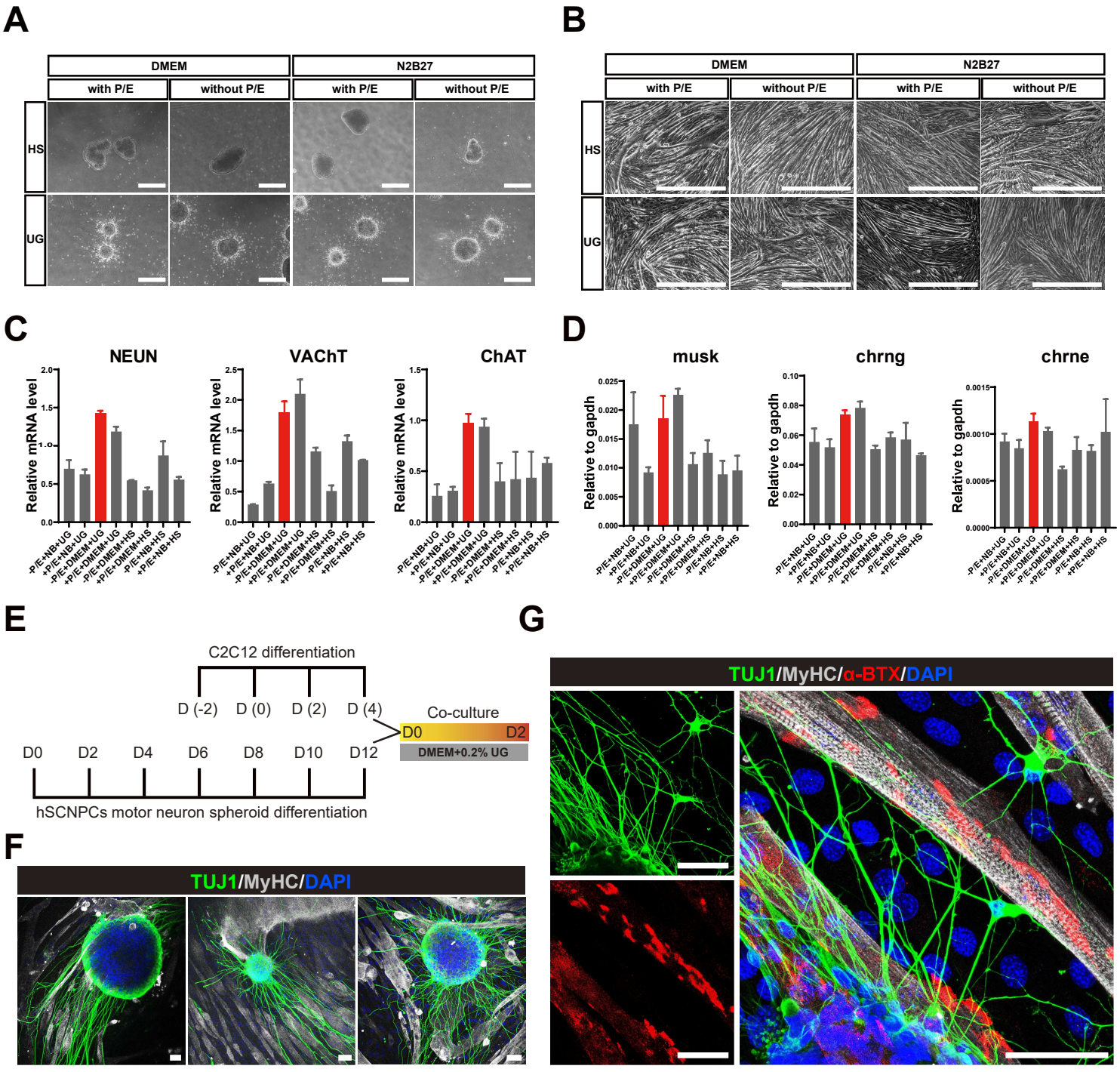

Figure S1. (Related to Figure 1)

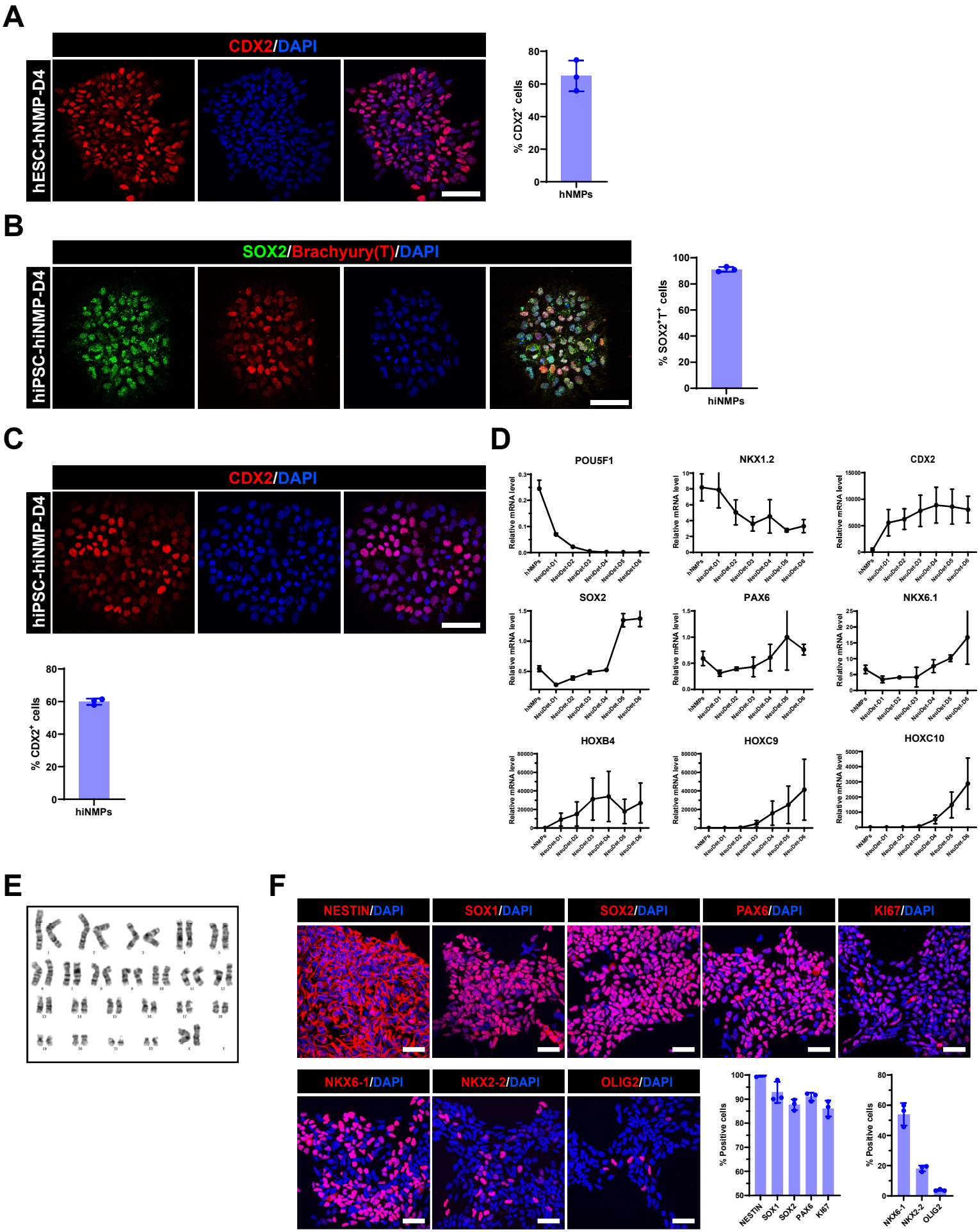

Figure S2. (Related to Figure 2)

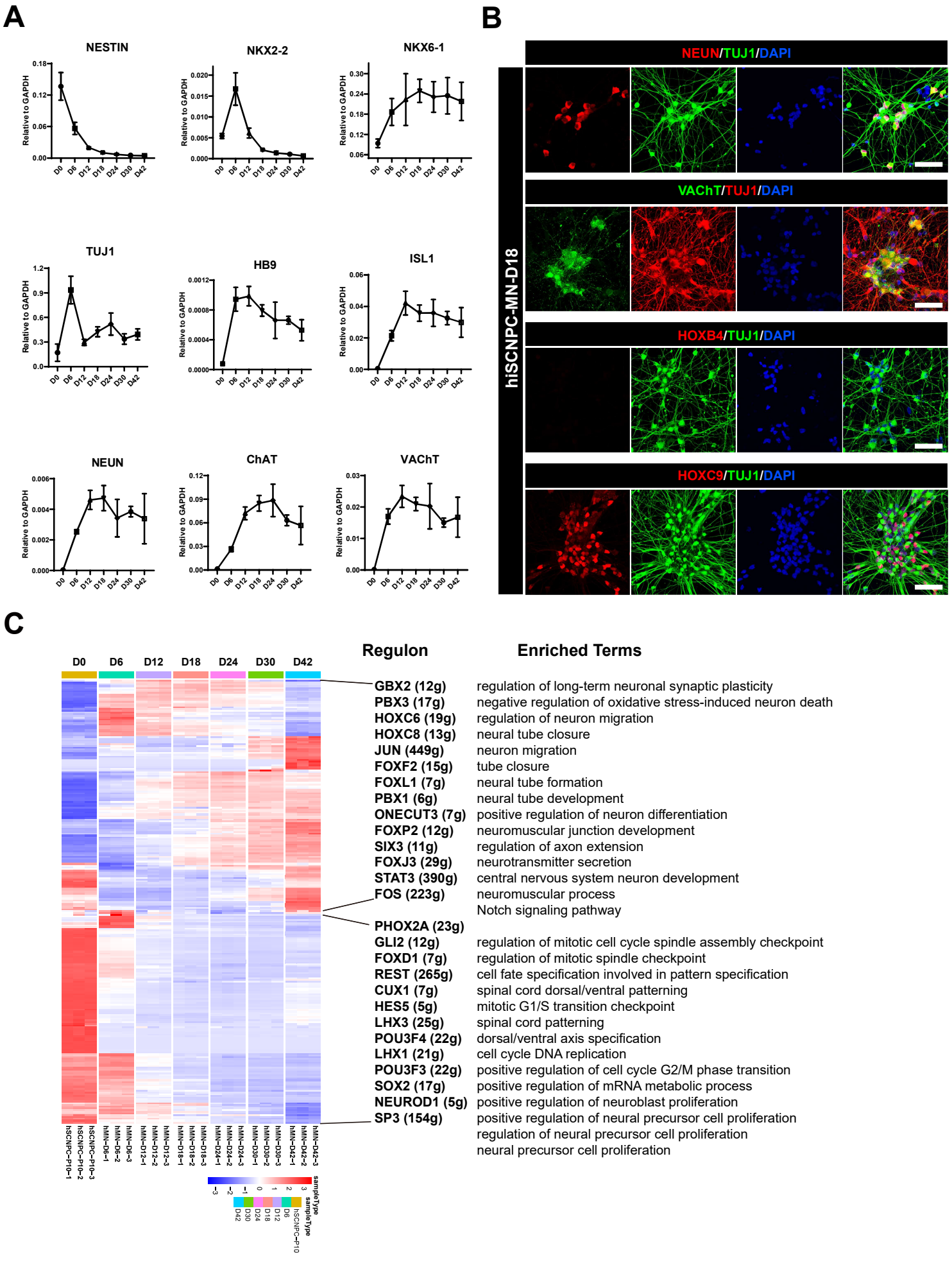

Figure S2. panel 2 (Related to Figure 2)

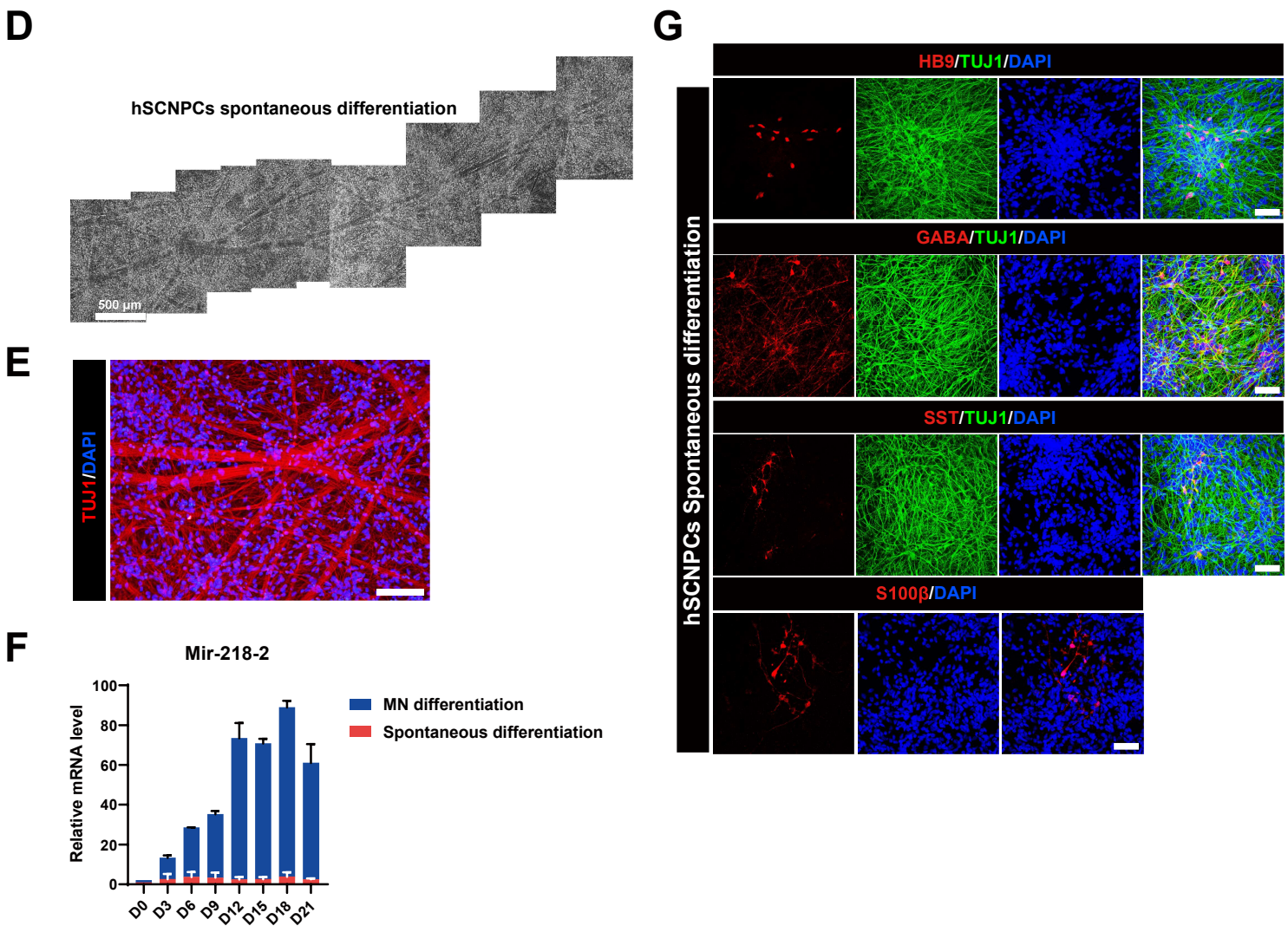

Figure S3. (Related to Figure 3)

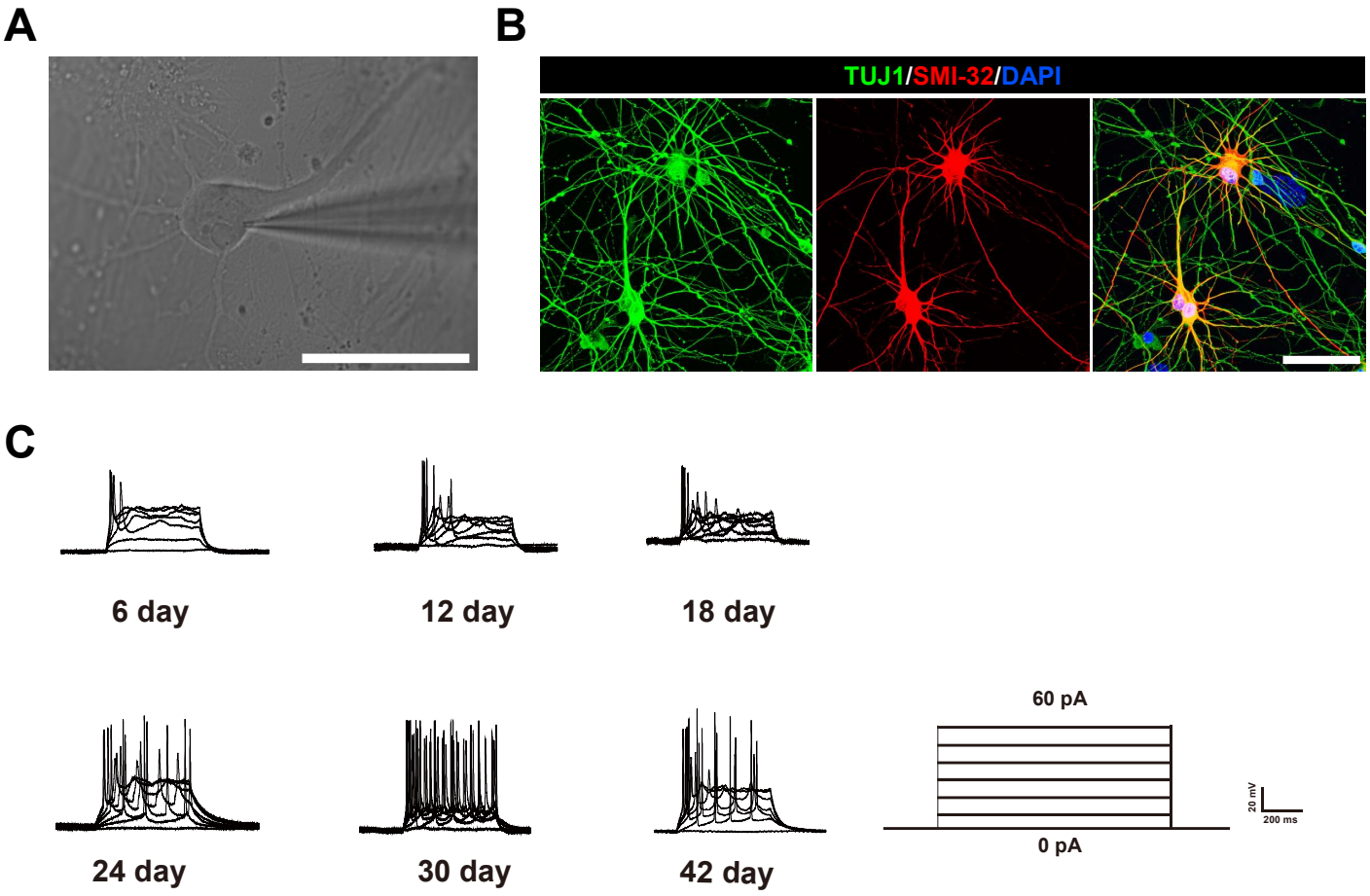

Figure S4. (Related to Figure 5)